Quarterly Journal of the Royal Meteorological Society

Q. J. R. Meteorol. Soc. 137: 137–155, January 2011

RMetS

Royal Meteorological Society

Processes driving deep convection over complex terrain: a multi-scale analysis of observations from COPS IOP 9c

U. Corsmeier,[a*] N. Kalthoff,[a] C. Barthlott,[a] F. Aoshima,[b] A. Behrendt,[b] P. Di Girolamo,[c] M. Dorninger,[d] J. Handwerker,[a] C. Kottmeier,[a] H. Mahlke,[a] S.D. Mobbs,[e] E.G. Norton,[f] J. Wickert[g] and V. Wulfmeyer[b]

[a]*Institute for Meteorology and Climate Research, Karlsruhe Institute of Technology (KIT), Karlsruhe, Germany*
[b]*Institute for Physics and Meteorology, University of Hohenheim, Germany*
[c]*Dipartimento di Ingegneria e Fisica dell'Ambiente, Università degli Studi della Basilicata, Potenza, Italy*
[d]*Department of Meteorology and Geophysics, University of Vienna, Austria*
[e]*Institute for Climate and Atmospheric Science, University of Leeds, UK*
[f]*School of Earth, Atmospheric and Environmental Sciences, University of Manchester, UK*
[g]*Department of Geodesy and Remote Sensing, German Research Centre for Geosciences, Potsdam, Germany*
*Correspondence to: Dr Ulrich Corsmeier Institute for Meteorology and Climate Research Karlsruhe Institute of Technology (KIT), Postfach 3640, 76021 Karlsruhe, Germany.
E-mail: ulrich.corsmeier@kit.edu

The 'Convective and Orographically-induced Precipitation Study' (COPS) analyses the processes driving deep convection over complex terrain. Convection initiation (CI) is mainly not only expressed by a single process, but by a variety of them, which interact on different scales in time and space and finally can lead to deep convection. A study of such a case over inhomogeneous terrain is presented in this article. Data from the COPS network of stations are taken to identify the time and location of CI. In many cases this is not the same location as the first convective clouds, showers or even thunderstorms. It is shown that the interaction of the CI processes on multiple scales locally leads to either deep convection and severe storms or calm weather. The boundary conditions between the different outcomes are narrow.

During IOP 9c (20 July 2007), a mesoscale convective system (MCS) embedded in a surface low over eastern France propagated north-eastward and a gust front of the MCS reached the COPS area. During the passage of the gust front through the Rhine valley, convective activity was significantly reduced. The gust front reached the slope of the Black Forest, and the warm and humid air above the mountain range prior to the gust front was lifted up to 2000 m within a short time period. Within the air prior to the gust front aloft from the surface, CI started along a north–south oriented line above the crest. Due to insolation ahead of the gust front, a convergence line developed. The interaction of local-scale orographic winds, the regional-scale gust front, the mesoscale convergence line, and the synoptic-scale cold front led to a squall line. Finally, individual severe convective cells formed along the outer section of the synoptic-scale cold front. Copyright © 2011 Royal Meteorological Society

1. Introduction

The initiation of deep convection is governed by large-scale mainly upper tropospheric processes as well as by regional and local-scale boundary-layer and soil-surface-driven processes. In cases of air mass convection, i.e. in the absence of air mass advection, the latter processes are frequent and dominant. In cases of large-scale forced convection, the

regional and local-scale processes can significantly modify the large-scale pattern of deep convection. Additionally, scale interaction of different circulation systems may cause rapid convective development depending on space and time. The focus of this paper is to investigate the influence of scale interaction between convection-initiating processes on the development of deep convection and subsequent convective precipitation. The CI processes investigated here are local wind systems, gust fronts, convergence lines, squall lines and synoptic-scale flow patterns.

Convection initiation (CI) is the beginning of atmospheric convection which may result in deep convection with severe weather like gust fronts, flash floods and thunderstorms. Therefore the conditions leading to CI are of great importance. It is necessary to include CI in nowcasting schemes as well as to represent CI in operational weather forecasting models. CI describes the processes which trigger coherent vertical motion of such strength that finally the level of free convection (LFC) is reached. Convection initiation, as defined in this article, is not visible in satellite and/or radar images, as it happens earlier, still in the (convective) cloud-free atmosphere. The interaction of convection-generating processes like orographic wind systems, moisture flux convergence, thermally direct circulations and mesoscale flow patterns is the prerequisite for CI. Due to the interaction of these processes on different scales, locally and temporally very high gradients of meteorological parameters (humidity, temperature, pressure, wind) develop in the lower troposphere, which are acting as a jump start for convection (Weckwerth, 2000).

Not all of the above-mentioned processes are subject to a diurnal cycle (e.g. large-scale processes, mesoscale convergence lines). Consequently, CI does not undergo a typical, repeatable diurnal cycle, unless a distinction is made between local-scale, surface or boundary-layer CI and large-scale CI. This makes it difficult to identify a diurnal cycle of CI. This paper examines when, where and why several interacting convection-initiating processes over complex terrain generate deep convection. This is done for the 'Intensive Observation Period 9c' (IOP 9c) dated 20 July 2007 of the 'Convective and Orographically-induced Precipitation Study' (COPS) performed from 1 June to 31 August 2007 in southwestern Germany and eastern France (Wulfmeyer *et al.*, 2008; Wulfmeyer *et al.*, 2011).

Numerous field campaigns have studied different convection initiation processes. In 2002, the International H_2O Project (IHOP_2002) was carried out in the southern USA over flat and gently rolling terrain. The focus was on surface-forced CI in cases of high convective instability with a strong capping inversion and its representation in weather forecast models. Special emphasis was put on mesoscale-alpha boundary layer circulations in the wind and humidity fields like frontal zones and drylines, which were considered responsible for triggering deep convection (Weckwerth *et al.*, 2004; Wilson and Roberts, 2006). Also, during the 2002 VERTIKATOR project (vertical exchange and orography) conducted over the low mountain range of the Black Forest in southwestern Germany, the magnitudes of humidity convergence and latent heat fluxes at the surface with respect to the orography were identified as decisive factors for the onset and intensity of convection and subsequent convective precipitation (Barthlott *et al.*, 2006; Meißner *et al.*, 2007).

A typical feature of the atmosphere prior to deep convection is the stable-layer phenomenon called a 'lid'

(Browning *et al.*, 2007). During the Convective Storms Initiation Project (CSIP, 2004 and 2005, United Kingdom), deep convection usually originated from elevated initiation processes in the atmospheric boundary layer, e.g. cold pools and cirrus shading, which is seen to be typical of this rather flat region (Marsham *et al.*, 2007). The 'lid concept' describes more-widespread CI conditions and it is less suitable for explaining convective conditions over low mountain ranges, which are governed by enhanced vertical motion and higher variability of the height of the planetary boundary layer (PBL) over time and space.

As shown by Koßmann *et al.* (1998) using TRACT data (TRansport of Air pollutants over Complex Terrain), the boundary-layer structure is influenced strongly by the underlying terrain in cases of negligible advection. At noon, a terrain-following capping inversion forced by horizontal convergence over the ridges develops, with high variability in PBL depth. The PBL inversion in the late afternoon tends to form a horizontal plane independently of terrain structure. During TRACT, valley winds were often found to result in mountain venting over the crests (Fiedler *et al.*, 2000). The influence of thermally driven secondary circulations like periodic slope and valley winds on CI is discussed by Koßmann and Fiedler (2000) and in Kalthoff *et al.* (2000) using TRACT data.

Conditional sampling techniques applied by Hasel *et al.* (2005) using data of a field campaign for the evaluation of atmospheric dispersion models (ESCOMPTE) performed in 2001 over a low mountain range and flat terrain in southern France revealed the importance of the underlying terrain to predominating structures within the PBL which might cause height variations of the PBL greater than terrain variability. Consequently, the PBL height variations depend on the size and vertical motion of the up- and downdraughts, transporting heat, humidity and momentum. Over the Black Forest during VERTIKATOR, conditional sampling clearly indicated the ascendancy of CI-generating large warm and moist updraughts in the centre level of the PBL (Hasel, 2006). This is a plausible sign for the existence of strong intermittent updraughts within the pre-convective environment generated by surface-layer convergence and finally resulting in moist convection.

Surface-based processes (e.g. sensible and latent heat fluxes) and secondary circulation systems (e.g. slope and valley winds) have been detected to be important features for the generation of moisture convergence and CI with subsequent deep convection. However, the question of why convection ensued where it did was still unanswered. This matter was investigated in the field campaign PRINCE (PRediction, Identification, aNd tracking of convective CElls, 2006) carried out in southwest Germany (Groenemeijer *et al.*, 2008). Besides the influence of an upper-tropospheric potential vorticity anomaly, a Doppler lidar revealed a local circulation over the slope of the dominating mountain in the pre-convective environment. Mass convergence was observed above the summit, resulting in vertical motion that locally broke the lid and was followed by the initiation of a precipitating convective cell. The PRINCE study demonstrated how a storm changed its own environment. A warm downdraught below the decaying parts of the storm caused a reduction of low-level moisture and warming in the lower troposphere that both reduced convective available potential energy (CAPE) and increased convective inhibition (CIN). This is important

for preventing subsequent convective development in the vicinity of the initial storm.

For COPS, a region with multi-scale orographic features with a high probability of CI and severe thunderstorm activity was selected. During COPS, a dense network of state-of-the-art instruments for atmospheric research was deployed in the area of investigation. These instruments were applied to the investigation of CI-related processes from the small scale to the mesoscale with variation in time and space. As shown by Kottmeier *et al.* (2008), surface and boundary-layer CI mechanisms (moisture convergence and scale interaction of convergence lines) and upper-level forcing (lifting) interact in many ways when convection is initiated. Case-studies with (i) local convection initiation over complex terrain, (ii) widespread convection triggered by lifting of potentially unstable air masses, and (iii) embedded convection at convergence lines and frontal zones explain the different CI mechanisms and their interaction as different chains of processes. Detailed studies by Kalthoff *et al.* (2009) and Behrendt *et al.* (2011) on COPS-IOP 8b investigate the initiation of convection by superposition of a synoptic-scale convergence and a regional-scale mountain range and thermally induced convergence. The dependence of convection-related parameters on surface and boundary-layer conditions over complex terrain during the COPS period was investigated by Kalthoff *et al.* (2011).

A study of statistics of CI by using Meteosat rapid scan data during COPS by Aoshima *et al.* (2008) clearly indicates the predominance of the low mountain sites of the Black Forest and the Vosges for the development of convection compared to the Rhine valley. In contrast to the article at hand, Aoshima *et al.* used a different CI definition based on cloud development. They found that convection over the mountains was three times as high as over the plain. Compared to the diurnal cycle, 18% of all CI cases took place over the mountains in a 1-hour interval about 2 hours after local noon.

Section 2 of this paper briefly summarises the COPS field phase. In section 3 the data of IOP 9c are analysed with respect to CI (i) on the synoptic scale, (ii) on the sub-synoptic scale, (iii) on the four-dimensional local scale, and (iv) with respect to the layering of the lower troposphere. The resulting precipitation patterns are discussed. Finally in section 4, the analysis is summarised and concluding remarks are given.

2. The COPS research initiative

The scientific goal of COPS is to advance the quality of forecasts of orographically induced convective precipitation by four-dimensional observations and modelling of its life cycle. An indispensable prerequisite for the simulation of convective precipitation is the understanding of mechanisms initiating deep convection over complex terrain. Important processes governing CI over complex terrain are reviewed by Kottmeier *et al.* (2008, Fig. 1: the large-scale scheme of CI) when discussing typical COPS cases with local, widespread and embedded convection and its initiation.

During COPS, a variety of airborne and ground-based remote sensing and *in situ* measuring instruments were operated to study the whole chain of processes from CI to convective precipitation. Five supersites were deployed in the COPS region (Wulfmeyer *et al.*, 2008, Figs 2 and 4: the network of instruments). The supersites were located along
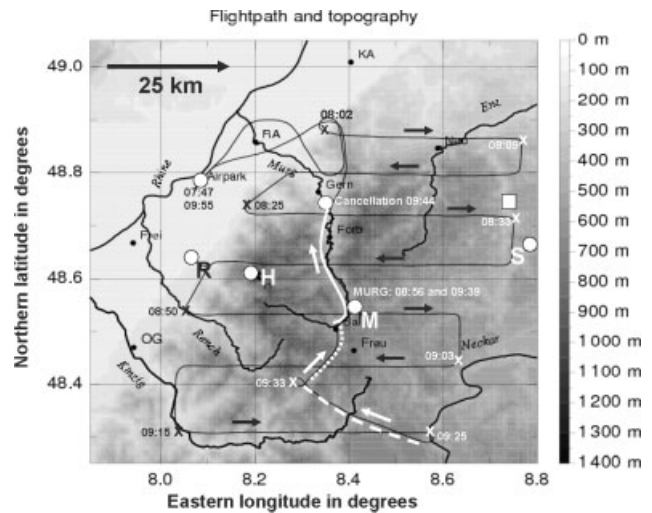

Figure 1. Orography of the inner COPS area over the northern Black Forest and the Rhine valley with supersites Rhine valley R (135 m amsl), Hornisgrinde mountain H (1163 m), Murg valley M (506 m), Stuttgart/Deckenpfronn S (550 m), and radiosonde station Calw-Hirsau (white square). Supersite Vosges V (150 m) is located outside the left margin. The flight pattern of the Do 128 aircraft is given by the black line and by waypoints (x) with timestamps. The direction of flight is indicated by the arrows. Take-off and touchdown at 'Airpark'. East−west legs are constant-level flights between 800 and 1400 m amsl. The white dashed line along the flight pattern indicates the southern ascent to 2950 m amsl, the dotted line the subsequent descending profile down to 900 m amsl, and the white line shows the low-level flight through the Murg valley from 900 to 600 m amsl. Main cities are: Karlsruhe (KA), Offenburg (OG), Freudenstadt (Freu) and Gernsbach (Gern).

a west−east cross-section through the COPS area in the low mountain region of the Vosges (V, 150 m amsl (above mean sea level)), in the Rhine valley (R, 135 m amsl), on top of Hornisgrinde, a summit of the northern Black Forest (H, 1163 m amsl), within the Black Forest's Murg valley (M, 506 m amsl), and in sloping terrain southwest of Stuttgart at Deckenpfronn (S, 500 m amsl) (Figure 1). Among others, these sites were equipped with lidar, differential absorption lidar (DIAL), sodar, cloud-radar, and UHF-radar wind profiler. Standard meteorological measurements were made and radiosondes were launched at up to 2-hourly intervals. A C-band radar at KIT, Campus North (10 km north of Karlsruhe, KA), for precipitation measurements provided information if and where convection led to precipitation. Research networks measuring the energy balance, turbulence and standard meteorological parameters were set up, and additional stations were installed to the operational Global Positioning System (GPS) network. Automatic weather stations were installed on top of the ridges and on the valley floors of the northern Black Forest to study in detail CI by local moisture convergence (Smith *et al.*, 2011, pers. comm.). Mobile teams in the field launched radiosondes prior to, during and after a convective cell passed the site. Meteosat-8 provided 5-minute rapid scans which were used to observe the evolution of convective clouds and to detect convection (Aoshima *et al.*, 2008). Aircraft were used for boundary-layer observations (Dornier Do 128 operated by the Technical University of Braunschweig and by KIT) and for mapping the large-scale flow conditions. Figure 1 depicts the orography of the inner COPS area of the northern Black Forest and the Rhine valley with the line of supersites R-H-M-S and the flight pattern of the Do 128 aircraft on 20 July 2007 during COPS IOP 9c, which is discussed in this article. The flight track is given by the black line and
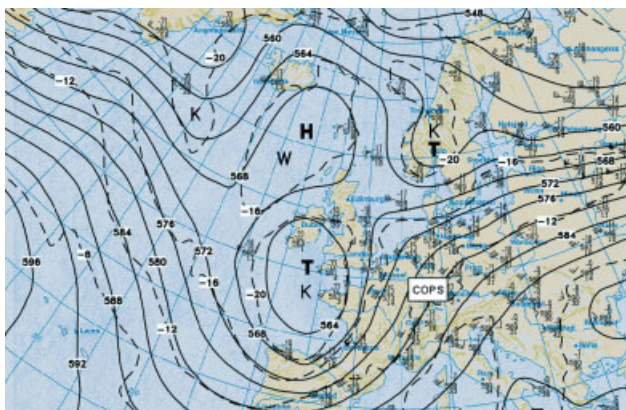
Figure 2. COSMO-EU analysis of the 500 hPa level with respective observations made for 20 July 2007, 0000 UTC. Black line: geopotential in gpdm; dashed line: temperature in °C; the outer COPS area is indicated.

by waypoints (x) with timestamps. The direction of flight is indicated by the arrows. Take-off and touchdown were at 'Airpark' (time indicated). East–west legs are at constant level between 800 m and 1400 m amsl. The white dashed and dotted lines along the flight pattern indicate the southern ascent to 2950 m amsl and the subsequent descent down to 900 m amsl. The continuous white line shows the low-level flight through the Murg valley from 900 m to 600 m amsl until the flight was cancelled due to severe weather. Main cities in the area are: Karlsruhe (KA), Offenburg (OG), and Freudenstadt (Freu). Details of the instruments and their deployment are given in the COPS field report (Wulfmeyer and Behrendt, 2007) and in Wulfmeyer *et al.* (2008) and Wulfmeyer *et al.* (2011).

3.   Analysis of observational data on different scales

The COPS IOP 9c case of 20 July 2007 is characterised by a sequence of interacting convection-triggering processes on different scales within a time period of about 12 hours. Starting with a mesoscale convective system (MCS) which generates several gust fronts staggered in time, one of these was modified by orographically driven thermal circulations and amplified by a convergence line, resulting in the initiation of secondary deep convection along the 'gust front – convergence line system'. In the end, a squall line with severe thunderstorms was generated (Kottmeier *et al.*, 2008). The COPS IOP 9c case was simulated using the WRF model by Schwitalla *et al.* (2011) and by Smith *et al.* (2011, pers. comm.).

3.1.   Organisation of convection on the synoptic scale

The synoptic-scale weather situation on 20 July 2007 at 0000 UTC on the 500 hPa level is dominated by a large-scale trough over western Europe and the eastern Atlantic, including a cold cut-off low south of the British Isles. As there is no phase shift between the geopotential wave and the temperature wave, the trough is quite stationary. The COPS area is located downstream of the trough in the transition zone to a weak ridge ranging from the Balkans to the North Sea (Figure 2). Downstream of the trough over France, the reduced surface pressure is widely around 1014 hPa, resulting in low wind speed. Warm and humid air lies over the Massif Central and the Mediterranean coast. Here, the

equivalent potential temperature Θ_e is up to 60°C, whereas Θ_e of below 40°C is measured over north-western France. The COSMO-EU model of the German Weather Service (DWD) expresses potential instability by the KO index as

$$KO = 1/2(\theta_{ps500} + \theta_{ps700}) - 1/2\,(\theta_{ps850} + \theta_{ps1000}) \quad (1)$$

with pseudo-potential temperature θ_{ps} on the levels of 500, 700, 850 and 1000 hPa. Values of $KO < -6$ K favour deep convection. The 0000 UTC analysis gives strong, but patchy instability with $KO < -12$ K over central France. Areas of lifting in the 500 hPa level of up to 14 hPa h^{-1} are found (not shown). These are favourable preconditions on the synoptic scale for widespread convection initiation even during the night. Figure 3 shows Meteosat-8 images of the infrared channel at 0000 and 0300 UTC. At midnight, one convective cell develops over central France. Within the next 3 hours, this cell rapidly grows, while others decline. At 0600 UTC, the anvil clouds of the storm cover the whole northeastern part of France. The cell has become an MCS with several updraughts in its centre, as traceable by the visible channel of Meteosat-8 (Figure 4, upper left). The location of the MCS corresponds to the significant maximum lifting of up to -45 hPa h^{-1} at 500 hPa analysed by COSMO-EU (not shown). Between 0000 and 0600 UTC, the centre of the MCS moves from central France to the area southeast of Paris. Here, the MCS reaches its peak level. From now on, a gust front generated by the downdraughts within the MCS forms a frontal structure moving eastward over the Vosges, the Rhine valley and the Black Forest. While passing different orographic structures and enhanced by radiative effects, i.e. fog in the Rhine valley (Figure 4, upper row) and clear sky east of the Rhine (Figure 4, lower left), the gust front is strengthened intermittently by thermally driven convergence on different scales between 0600 and 1200 UTC. At the beginning, the gust front initiates convective clouds west of the Vosges which are visible between 0615 and 0745 UTC directly east of the MCS's core (Figure 4, top right). After a 30-minute period of retrogression of clouds, a new convective development takes place between 0815 and 0900 UTC when the gust front propagates over the Vosges (Figure 4, lower left). Within the next 30 minutes, the gust front passes the Rhine valley, an approximately 40 km wide flat area (150 m amsl) between the low mountain ranges of the Vosges (west) and the Black Forest (east), both with summits of up to 1500 m amsl. Prior to the passage of the gust front, the fog within the valley dissolves due to increasing wind speed and mixing. The convective clouds mostly disappear when the gust front descends into the valley. At 0930 UTC, the gust front reaches the western slope of the northern Black Forest. When climbing up to ~1100 m amsl between supersites R and H (Figure 1), new low-level clouds are formed at the head of the gust front. When the gust front passes the summits of the Black Forest, CI takes place by moisture flux convergence and rapid lifting of the air mass prior to the gust front (details shown later). The development in the COPS area ends at noon with the generation of a squall line with thunderstorms and heavy precipitation east and north of the Black Forest (Figure 4, lower right). Within 12 hours, a development from an MCS to a cold front with an embedded squall line has taken place by interacting processes on different atmospheric scales.
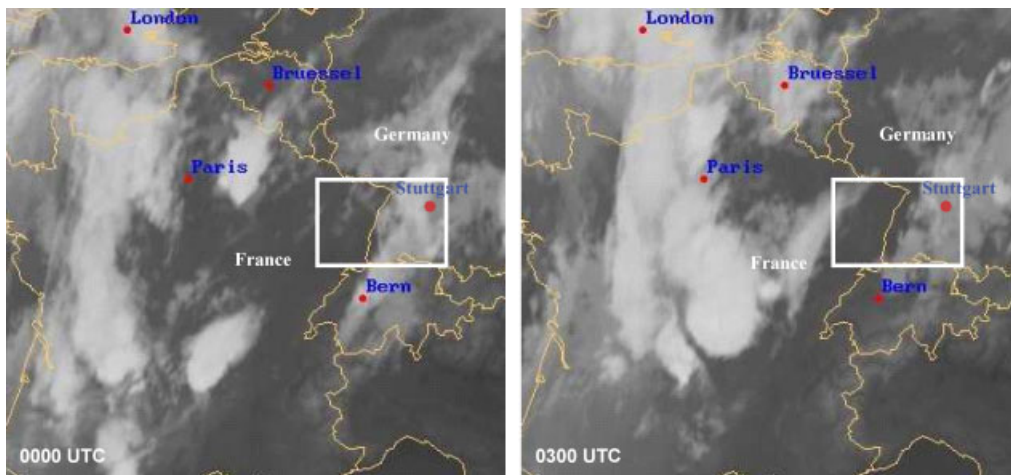
Figure 3. EUMETSAT Meteosat-8 satellite images (infrared channel) from 20 July 2007, 0000 and 0300 UTC. The outer COPS area is indicated by the white frame. This figure is available in colour online at wileyonlinelibrary.com/journal/qj
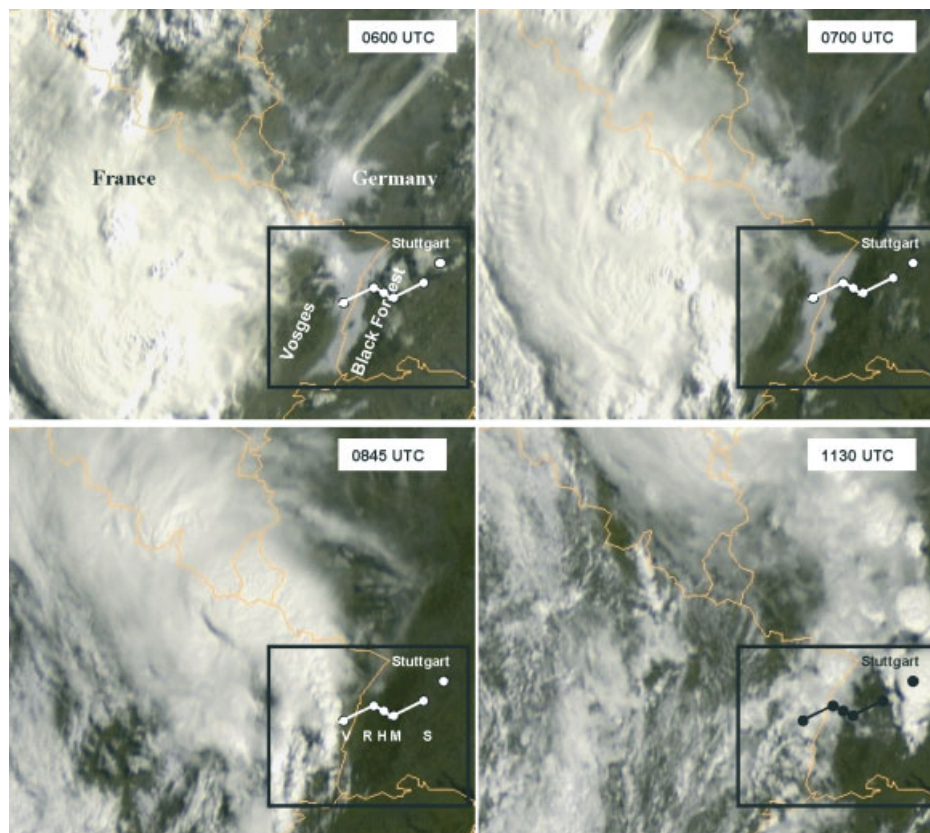

Figure 4. EUMETSAT Meteosat-8 images (visible channel) from 20 July 2007: 0600, 0700, 0845 and 1130 UTC. The outer COPS area with the line of supersites V-R-H-M-S is indicated by the black frame.

3.2. Surface observations on the sub-synoptic scale

For the interpretation of the night-time convective development upstream of the COPS area, the 'Vienna Enhanced Resolution Analysis' (VERA) is used (Steinacker *et al.*, 2006). All observations available from weather services, official and private sources are taken, checked for their quality, and interpolated on an 8 km grid. Secondary data are calculated on this basis. In this case, many features of mesoscale convective systems as discussed by Browning and Ludlam (1962) could be identified. Figure 5 displays the VERA wind field (10 m above the soil surface) and the surface pressure. At 0000 UTC, a weak surface low without

recognisable fronts ($p < 1013$ hPa in the Paris area) and with very weak wind is located over France downstream of the 500 hPa trough. At the location of the initial MCS development over southern France, a backward inflow into the system is found (Figure 5, upper left). At 0300 UTC, this convective system moves northward and the anvil clouds spread out (Figure 3, right). Ahead of the convective cell to the north and northeast, the westerly wind increases, which might indicate an outflow, while at the back, the westerly flow is reduced by the outflow (Figure 5, upper right). The centre of the surface low moves northward as well, and its core pressure decreases below 1012 hPa. Three hours later (0600 UTC), the MCS is fully developed. It moves

north-eastward and, at the leading edge of the convective core, an outflow of up to 3 m s^{-1} is measured, while west of the cell the wind is still very weak. The core of the low near Paris moves further northward to the Channel and its pressure is now < 1011 hPa (Figure 5, lower left). During the next 3 hours, the centre of the low moves north-westward to southern England and the MCS propagates in a north-easterly direction. While the horizontal wind speed is near zero under the core of the cell, downstream a pronounced north–south oriented gust front develops over the Vosges. The wind speed is 7 m s^{-1} and the length of the gust front is 160 km (Figure 5, lower right). Time (0700 to 0900 UTC) and location (west of the Vosges summits) of the most developed gust front correspond well to the two stages of convective clouds in Figure 4 (0700 and 0845 UTC).

Near the surface, the horizontal gradient of the equivalent potential temperature Θ_e at the eastern edge of the MCS is significantly enhanced by the developing and propagating gust front between 0600 and 0900 UTC. While at 0600 UTC typical values of 1 to 2 K/100 km are found over the French COPS area, the gradient increases to 12 K/100 km in the COPS area east of the MCS at 0900 UTC (Figure 6, upper panel), indicating the increasing difference between the dry and cold MCS downdraught and the warm and humid air downstream (north and east) of the MCS. This finding corresponds to the curvature of the 1014 hPa and 1013 hPa isobars below the MCS, displaying a higher pressure at the back left-hand side and lower pressure at the front right-hand side of the MCS, seen in the direction of its propagation in Figure 5. At 0900 UTC, a local high-pressure centre (1015 hPa) develops at the back of the MCS, as described by Kurz (1990) (Figure 5, lower right). The MCS roughly propagates with the mid-tropospheric wind speed of about 60 km h^{-1}. At 1000 UTC, a further increase of the horizontal Θ_e gradient up to 28 K/100 km in a west–east direction almost perpendicular to the crest of the northern Black Forest is found (Figure 6, lower left). This is where the gust front is lifted by the orography and a thermally direct circulation is triggered, both favouring CI over the crest within the warm and humid air prior to the gust front (small-scale analysis given later). At 1200 UTC, the gradient of Θ_e in this mountainous area is reduced to 5 K/100 km due to strong vertical exchange by deep convection over the last two hours (Figure 6, lower right).

The corresponding scheme of moisture flux divergence at 0800 UTC depicts negative values (convergence) at the leading edge of the gust front reaching the western slope of the Vosges of −70 g kg^{-1}s^{-1} as visible in Figure 7 (upper left). A second moisture flux divergence maximum of −60 g kg^{-1}s^{-1} is identified over the western slope of the northern Black Forest. This maximum is found from 0300 UTC and is not related to the MCS, which is still too far away in the west. The maximum is associated with the easterly flow in this area, the circulation around the northern Black Forest, and the corresponding channelling in the Rhine valley (Kalthoff and Vogel, 1992). At 0900 UTC, the moisture flux divergence increases to more than −80 g kg^{-1}s^{-1} in this area and to more than −50 g kg^{-1}s^{-1} in the Rhine valley due to the gust front arriving from the Vosges. At 1000 UTC (Figure 7, lower left), the gust front climbs the western slope of the Black Forest and the two moisture flux convergence maxima merge, to a line-like convergence of −150 g kg^{-1}s^{-1} over the northern Black Forest and to −70 g kg^{-1}s^{-1} further to the south.

At the same time, the moisture flux at the Black Forest's western foothills changes to divergence of 40 g kg^{-1}s^{-1}, indicating a narrow band of convergence just over the hills. Upstream over the Vosges, a similar but weaker moisture divergence–convergence pattern is analysed. At 1100 UTC, the thermally driven convergence line in the eastern COPS area and the dynamically induced gust front interact by lifting the air prior to the gust front (shown later). At the same time the strongest moisture convergence is observed in a north–south orientation over the Black Forest with −110 g kg^{-1}s^{-1} in the north, where CI starts around 1000 UTC (shown later), and −80 g kg^{-1}s^{-1} in the south (Figure 7, lower right).

Figure 8 shows the final synoptic-scale conditions, after the transformation of the MCS into a weak lower tropospheric cyclone. The cyclone is located downstream of the mid-tropospheric trough with its centre over western Germany, the Netherlands and southeastern United Kingdom. It is a fully developed frontal system, with a line of convective cells (squall line) along the convergence line. Between 0600 and 1200 UTC, the developing cold front is strengthened in sections by the gust front. Differences in the short-wave radiation on both sides of the gust front form a convergence line ahead. The gust front moves eastward far into the COPS region. Triggered by the interaction of different-scale secondary circulation systems at the convergence line, a squall line with a number of thunderstorms stretching from the COPS region to the north and northwest along the cold front is formed (Figure 8, DWD precipitation radar composite). The southernmost and biggest convective cell is initiated near the summits of the northern Black Forest hills ∼2 hours before (1000 UTC). The reasons for its formation are manifold: (i) the gust front originating from the MCS propagating at high speed to the east initiating lifting and an increasing horizontal temperature gradient, (ii) lifting of up to 1000 m caused by the Black Forest hills, (iii) the generation of converging valley and slope wind systems at the low mountain range (Smith *et al.*, 2011, pers. comm.), and (iv) the effect of prefrontal heating of the surface by high solar insolation during the forenoon on the formation of a prefrontal convergence zone. The interacting convection-initiating processes are explained by data analysis on the local scale.

3.3.   Surface analysis on the local scale

At the surface, the propagation of the gust front and the development of the convergence line can be identified by temperature and wind measurements between 0700 and 1200 UTC (Figure 9). At 0700 UTC (top left), the near-surface temperature in the whole COPS area is between 16 and 22°C and the wind is up to 5 m s^{-1} from easterly directions. Only in the southwest, near the MCS (Figure 4, upper right), is a westerly wind measured. In the Rhine valley below the fog, the wind is calm and the air temperature is uniformly 18°C. At 0900 UTC, downdraughts of cold (16 to 18°C) and moderately dry air (10 g kg^{-1}, not shown) spread out like a circle from the secondary convection generated by the MCS over the Vosges (Figure 4, lower left). Strong westerly winds of up to 8.0 m s^{-1} dissolve the fog in the Rhine valley. After passing the valley between 0900 and 1000 UTC, the line of strong wind is deformed by orographic effects. The head of the gust front (Figure 9, top right, red line) reaches the western slope of the Black
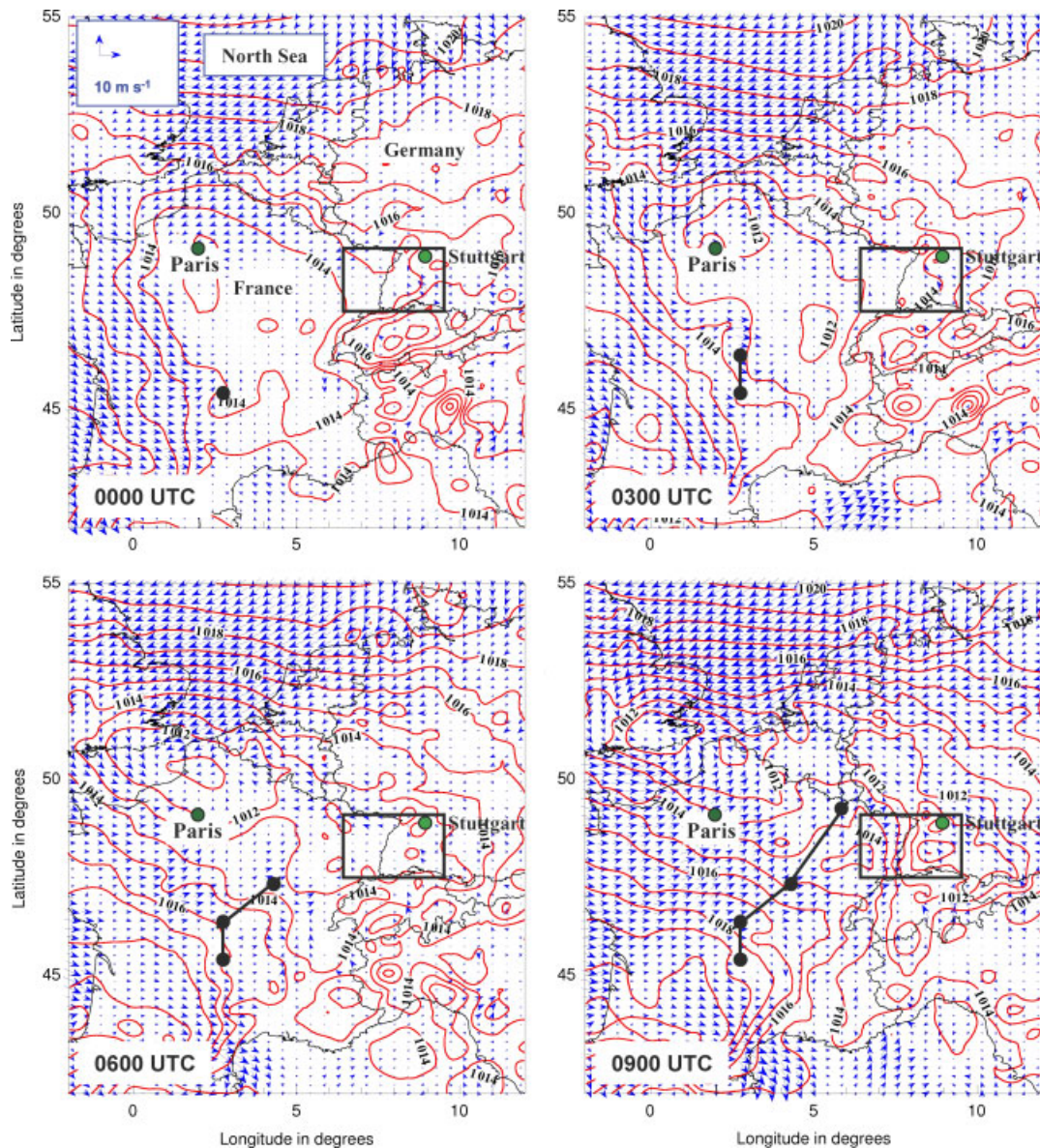
Figure 5. Analysis of observed surface wind in m s^{-1} (arrows) and surface pressure in hPa reduced to msl (isolines) for 20 July 2007 at 0000, 0300, 0600 and 0900 UTC using the VERA analysis and interpolation method on an 8 km grid. The outer COPS area is indicated by a rectangle, and the position and track of the core cell of the MSC is given by black dots and lines. This figure is available in colour online at wileyonlinelibrary.com/journal/qj

Forest between Strasbourg and Karlsruhe at 0915 UTC (Kinzig valley entrance, Figure 1) and at 0940 UTC (Murg valley entrance, Figure 1). Low-level clouds form between supersites R and H (Figure 1) with a cloud base of 0 m above ground level (agl) above 300 m terrain height; the gust front ascends to the summits of the Black Forest and reaches supersite H at 0933 UTC. This is visible by the wind speed increase from 2.0 to 6.4 m s^{-1} within 3 minutes and turning of the wind direction from east-southeast to west, followed by a temperature decrease (Figure 10, upper panel) within 30 minutes from 22.5°C down to 14.5°C. While propagating further east, the gust front at 0955 UTC is detected above the supersite M (Murg valley, Figure 1), as reflected by vertical wind, temperature and humidity profiles from lidar and a microwave radiometer, and by wind profiles from a four-instrument sodar network in the area (not shown).

At 1003 UTC, the gust front reaches Freudenstadt, 22 km southeast of supersite H. This results in a propagation speed of the front of 12.2 m s^{-1}. The temperature decrease at Freudenstadt is 5.5°C and wind turns from easterly to

westerly. Now, the leading edge of the gust front is located over the northern Black Forest and is shaped like an arch of approx. 25 km width. Karlsruhe in the north and Freiburg in the south are excluded (Figure 9, lower left). The mean wind speed behind the gust front is about 7 m s^{-1} coming from the northwest and the temperature is 20°C or even less. Ahead of the gust front, the wind direction still is southeasterly and the air temperature increases up to 28°C in the Stuttgart area. The direction and speed of propagation of the gust front is significantly modified by the main valleys of the rivers Murg, Enz, Rench and Kinzig (Smith *et al.*, 2011, pers. comm.).

While propagating further eastward, the gust front reaches the supersite S (Figure 1), halfway between Freudenstadt and Stuttgart, at 1030 UTC. This is indicated by the turning of the wind from east-southeast to west-southwest, an increase in the mean wind speed from 2.5 to 7.0 m s^{-1}, and a decrease of the temperature from 28°C down to 20°C (Figure 10, middle). The humidity at this site decreases by 3 g kg^{-1} after the passage of the gust front. This is in contrast to supersite
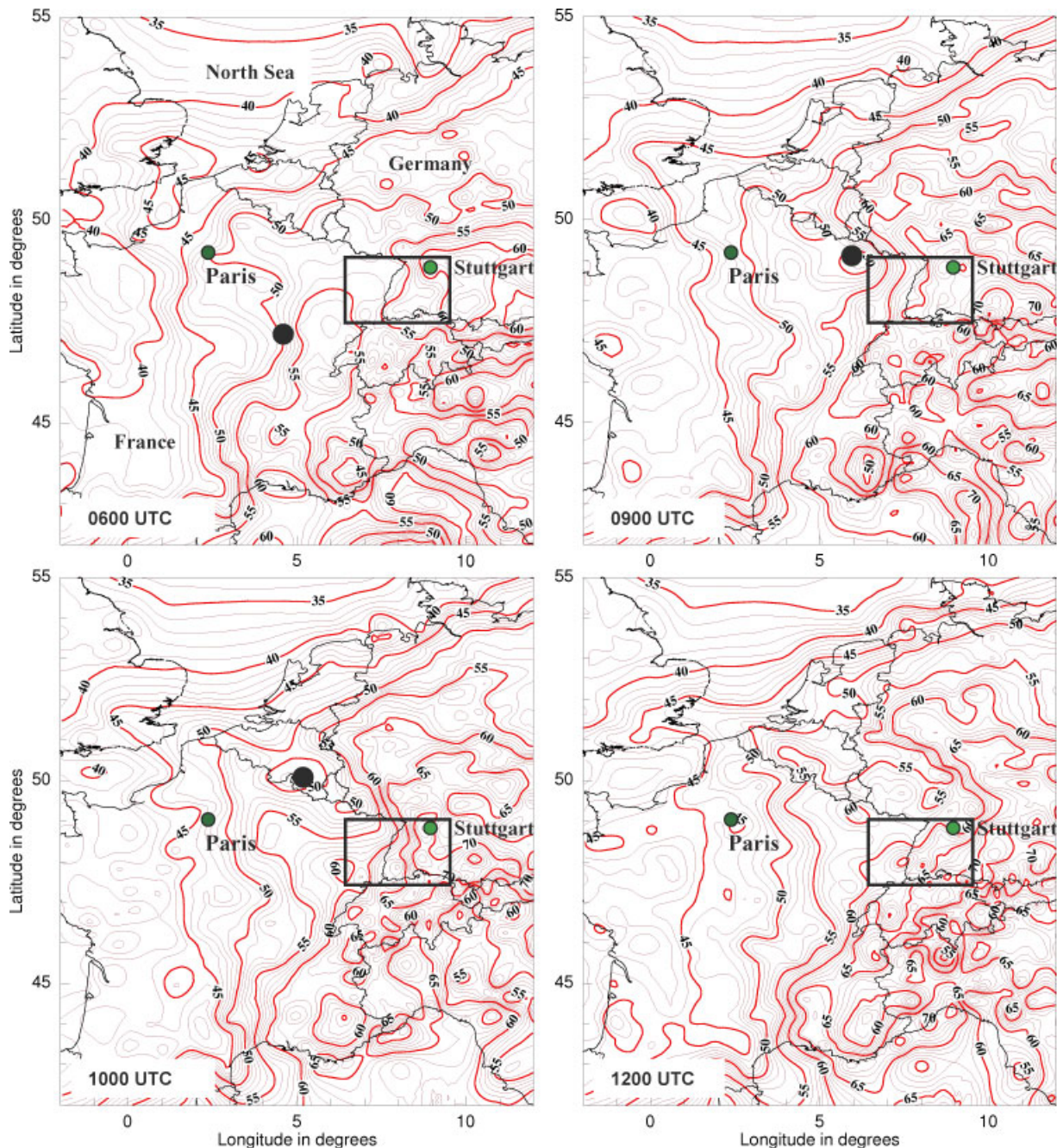
Figure 6. VERA-calculated fields of equivalent potential temperature Θ_e in °C from surface observations on 20 July 2007 at 0600, 0900, 1000 and 1200 UTC. The outer COPS area is shown by the black rectangle, and the core cell of the MSC is given by black dots. This figure is available in colour online at wileyonlinelibrary.com/journal/qj

H where little change of humidity was observed. As shown later, the humidity reduction behind the gust front near the surface is widespread. Supersite H is an exception, because the clouds of the gust front head reach the surface at this site during the passage. Between Freudenstadt and Stuttgart, the speed of the front accelerates to approx. 17 m s^{-1}.

Two hours later, at 1200 UTC, the situation has changed significantly (Figure 9, lower right). The temperature in the Stuttgart area and south of it over the Swabian Jura reaches 28 to 30°C or higher. Over the northern Black Forest, the air temperature is about 18°C. These differences are caused by cloud shading (Figure 4, lower right) and the cold air behind the gust front, which is now flooding the northern Black Forest exclusively. Strong westerly wind in the cold air over the Black Forest and little easterly wind in the warm

air of the Stuttgart area result in an enhanced horizontal temperature gradient and subsequently cause subsidence of the cold air and lifting of the warm air. This results in a thermally driven direct circulation with the development of a convergence line. The line is located along the red line in Figure 9. The three southernmost cumulonimbus clouds in Figure 8 (inserted radar image) indicate the position of the convergence line at 1200 UTC. At this time, the structure of the convergence line increasingly changes to a squall line dominated by individual cells of deep convection (Figure 10). At 1115 UTC, the gust front arrives at Stuttgart with a speed of 11 m s^{-1}, the temperature decreases from 29.5 to 22.0°C and the humidity is reduced by 2.5 g kg^{-1}. The wind turns from southeast to west and accelerates from 3 to 13 m s^{-1}. However, the passage of the gust front takes
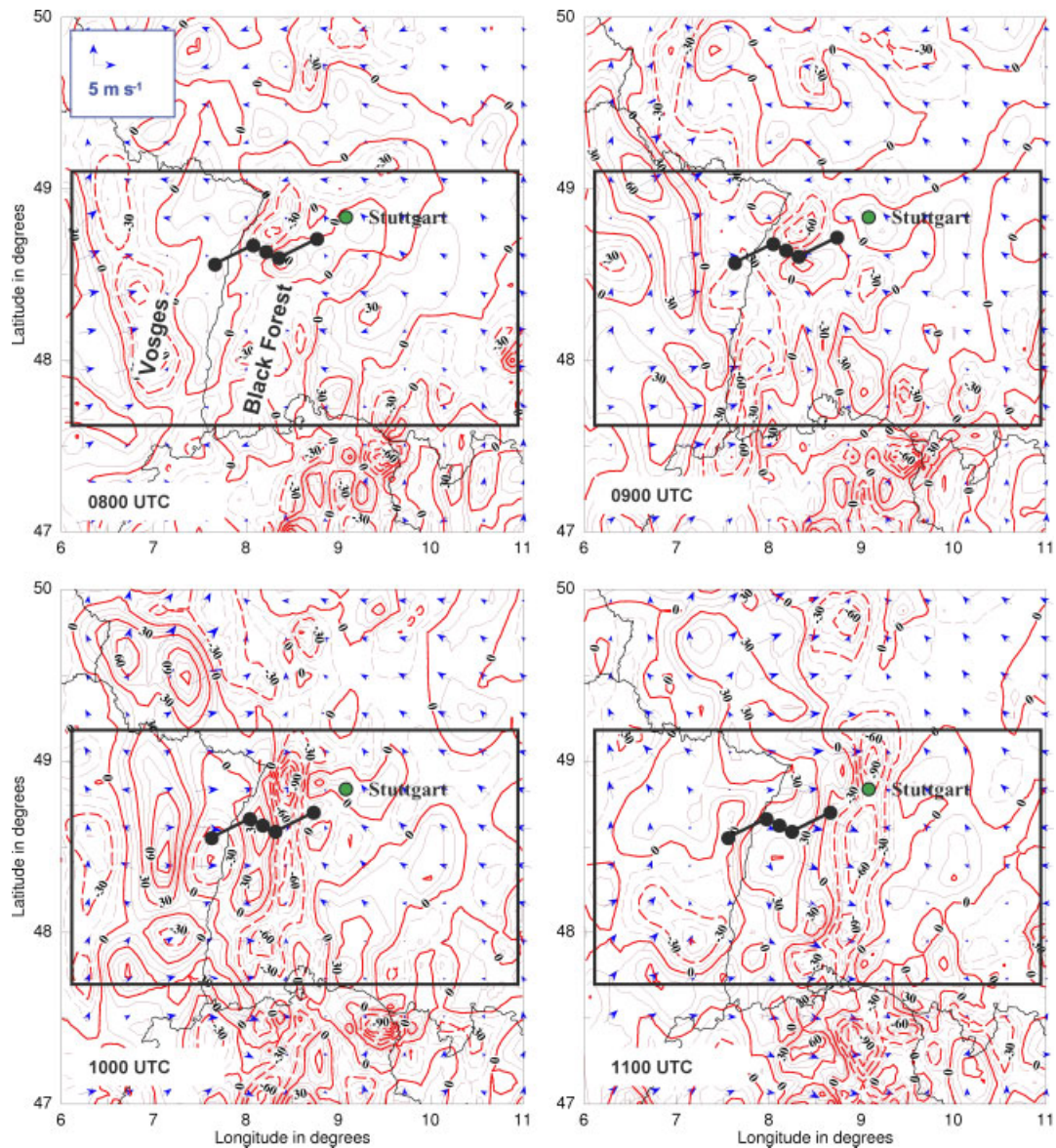
Figure 7. VERA-calculated moisture flux divergence (solid lines) and convergence (dashed lines) in g kg^{-1}s^{-1} from surface observations for 20 July 2007 at 0800, 0900, 1000 and 1100 UTC. The outer COPS area with the line of supersites V-R-H-M-S (black dots, from west to east) is indicated by the black rectangle. This figure is available in colour online at wileyonlinelibrary.com/journal/qj

only about 60 minutes. At 1300 UTC, the wind turns back to easterly and the wind speed is reduced to 2 m s^{-1}. At 1515 UTC, a turn to westerly again with an acceleration of the speed is measured at Stuttgart, which reflects the arrival of the cold front behind the convergence line and gust front. The transformation of the convergence line – gust front system into a squall line with individual convective cells and the corresponding wind field can be studied in Figure 10 (left panel) on the way from supersite H over S to Stuttgart. From west to east, the maximum wind speed increases, but the time frame with wind from westerly directions is reduced. This confirms the formation of an individual circulation system within the line.

The humidity field near the surface does not show such a significant change when the gust front passes. The specific humidity in the COPS area is between 9 and 14 g kg^{-1} before the passage. Behind the gust front, the humidity is slightly reduced by approximately 1 g kg^{-1} in the Rhine valley and by 2 g kg^{-1} over the Black Forest (not shown). These findings are in contrast to the integrated water vapour

(IWV) data measured by a network of GPS receivers in the COPS area. Figure 11 shows the measured and interpolated IWV data which are dominated by the water vapour in the lower troposphere. Between 0900 and 1100 UTC, the IWV increases in the Rhine valley from 31 to 38 kg m^{-2} and over the mountains from 24 to 33 kg m^{-2}. Except for the surface layer, humidity increases behind the gust front in the boundary layer and the lower troposphere due to advection of a narrow, elongated humidity belt. This results in stability modifications of the atmosphere.

3.4. Atmospheric stability and convection initiation

The passage, vertical extension and cloud structure of the gust front are documented by the synergy of remote-sensing instruments. The Facility for Ground-based Atmospheric Measurements (FGAM) ultra high frequency (UHF) radar wind profiler (Norton *et al.*, 2006) provided wind profiles and the University of Basilicata Raman lidar (Di Girolamo *et al.*, 2009) measured profiles of the range-corrected signal
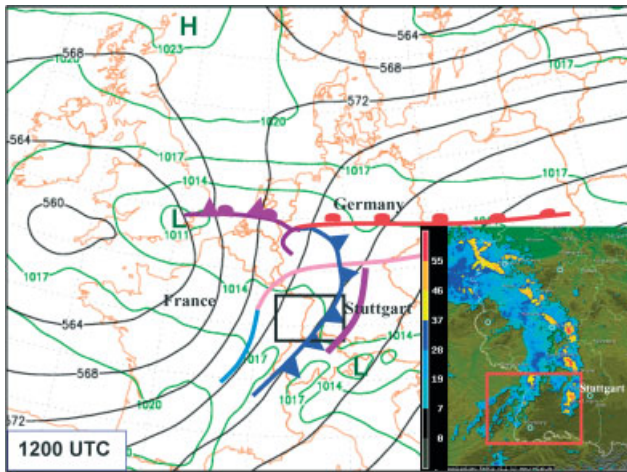
Figure 8. COSMO-EU model analysis of the surface pressure in hPa (green) and the 500 hPa level in gpdm (black) for 20 July 2007, 1200 UTC. The 1200 UTC surface fronts including the convergence line are indicated by dark colours (violet, dark blue, red). The positions of the fronts at 0600 UTC are given in light colours (pink and pale blue). The inserted figure shows the reflectivity in dBZ at 1111 UTC as measured by the DWD radar network. Convective cells at the convergence line can be identified by high reflectivity (yellow, red). The COPS area is indicated by the rectangles.

at 1064 nm and water vapour mixing ratios at supersite R, 12 km downslope of supersite H (Figure 1). Figure 12 (top panel) shows profiles of horizontal winds from the UHF wind profiler. The wind speed is shown by the colours and the direction shown by the arrows. The arrival of the gust front at 0925 UTC is indicated by a turning of the wind to westerly and increasing wind speed of 15 m s^{-1}. Simultaneously the vertical wind speed increased up to 1.5 m s^{-1} (2nd panel). This was about 8 minutes earlier than at supersite H, resulting in a propagation speed of the gust front of 25 m s^{-1}, which is twice as fast as the speed found later over the mountains. The vertical motion behind the gust front is characterised by four periodic upwind maxima between 0925 and 1005 UTC. The vertical extension of the slightly tilted gust front in the Rhine valley is about 1000 m and it is accompanied in the lowest layer by a cloud with base near the surface at its leading edge (Figure 12, 3rd panel, section A) and high humidity (lower panel). After the cloud head has passed the site, a 15-minute interval of clear sky and reduced humidity is observed (section B), before a new line of very low clouds and high humidity passes the site between 0945 and 1000 UTC (section C). Around 1015 UTC, the site R is quite free of low clouds (section D), and at 1030 UTC convective clouds with showers are detected at supersite R (2nd panel, 3rd panel section E). After the gust-front passage (0925 to 1100 UTC), the depth of the air mass characterised by westerly wind increases from 1000 to 2000 m (top panel). A cloud layer in the shear zone above the westerly winds rises simultaneously (3rd panel), but the layer of highest wind speed up to 15 m s^{-1} is fixed between 200 and 1200 m amsl (top panel). Within this layer, increasing humidity is detected in section D from 1000 to 1025 UTC (lower panel) which is in accordance with an increase of humidity in the lower troposphere detected by the GPS network (Figure 11). After 1100 UTC, the gust front influence decreases, as the wind turns to southwesterly according to the synoptic-scale flow.

Figure 13 explains the vertical stratification between 0530 and 0930 UTC prior to the gust front at the summit supersite H. Vertical profiles of mixing ratio and temperature

above 500 m agl are deduced from the water vapour DIAL (Wulfmeyer and Bösenberg, 1996; Behrendt *et al.*, 2009) and rotational Raman lidar (Radlach *et al.*, 2008) measurements. The resulting lifting condensation level (LCL) and the LFC are calculated by additional measurements from near the surface, leading to an estimate of buoyancy *B* in the lower 6000 m of the troposphere. *B* is calculated by

$$B = g \left(\Theta_{\text{parcel}} - \Theta_{\text{ambient}} \right) / \Theta_{\text{ambient}} \qquad (2)$$

The LCL is estimated to be approximately between 600 and 950 m above the summit during the four hours of observation. This is on average a little less than the LCL calculated by the 0808 UTC radiosonde (Table I). The LCL height variation in time is mainly due to the difference between near-surface temperature and dew-point. The LFC decreases from an average of 2200 m agl at 0545 UTC to about 1100 m agl at 0845 UTC. This results in an increase of buoyancy above the LFC. The decrease of the LFC is attributed to the increasing absolute values of surface temperature and humidity at constant difference.

The depth of the cold and humid air mass behind the gust front at supersite H is restricted to the lowest 1800 m agl (3000 m amsl), as deduced from vertical profiles of three radiosondes (Figure 14). Between the two soundings at 0808 and 1113 UTC, the temperature decreases by 7°C in this layer and the humidity increases by 5 g kg^{-1} between 800 and 1800 m agl. However, between the first two soundings at 0508 and 0808 UTC in the lowest 500 m agl, the humidity increases by 3 g kg^{-1}. The wind accelerates from 10 to 15 m s^{-1} at 400 m agl and turns from south-southeast to west between 0808 and 1113 UTC. This coincides well with the UHF radar wind profiler data from supersite R (Figure 12), taking into account the forced lifting of the air mass when ascending the slope. The high CAPE of 717 J kg^{-1} at 0808 UTC (Table I) favours the intensity of convection at supersite H (if initiated by low CIN) within a short period prior to the passage of the gust front, followed by a slot of suppressed convective conditions (1100 until 1200 UTC). So convection could have been started, if (i) the convective temperature T_c was reached, and/or (ii) lifting was triggered by local convergence, and/or (iii) lifting was forced by the orography. It will be shown that orographic lifting, followed by free convection over the westernmost crest of the Black Forest plays the primary and decisive role in the initiation of convection, which finally leads to deep convection with severe thunderstorms more than two hours later far to the east in the Stuttgart area.

Figure 15 shows a sequence of C-band radar reflectivity images each in a horizontal plane and two vertical planes between 1000 and 1135 UTC. The radar is located 10 km north of Karlsruhe (Figure 1). Before 0915 UTC, prior to the gust front arrival, the Black Forest is completely free of clouds. At 1000 UTC, an approximately 60 km long and north–south oriented line of precipitating convective cells of up to 10 km height formed rapidly between the western crest of the Black Forest (supersite H) and the Murg valley (supersite M) (Figure 15, upper left). The very first showers are detected at 1000 UTC at a height above 4000 m amsl which is 2800 m above Hornisgrinde (upper left x–z plane). That means that CI must have happened earlier. The developing line of convective cells moves eastward parallel to the gust front propagation at the surface (Figure 9). The cells develop rapidly with cloud
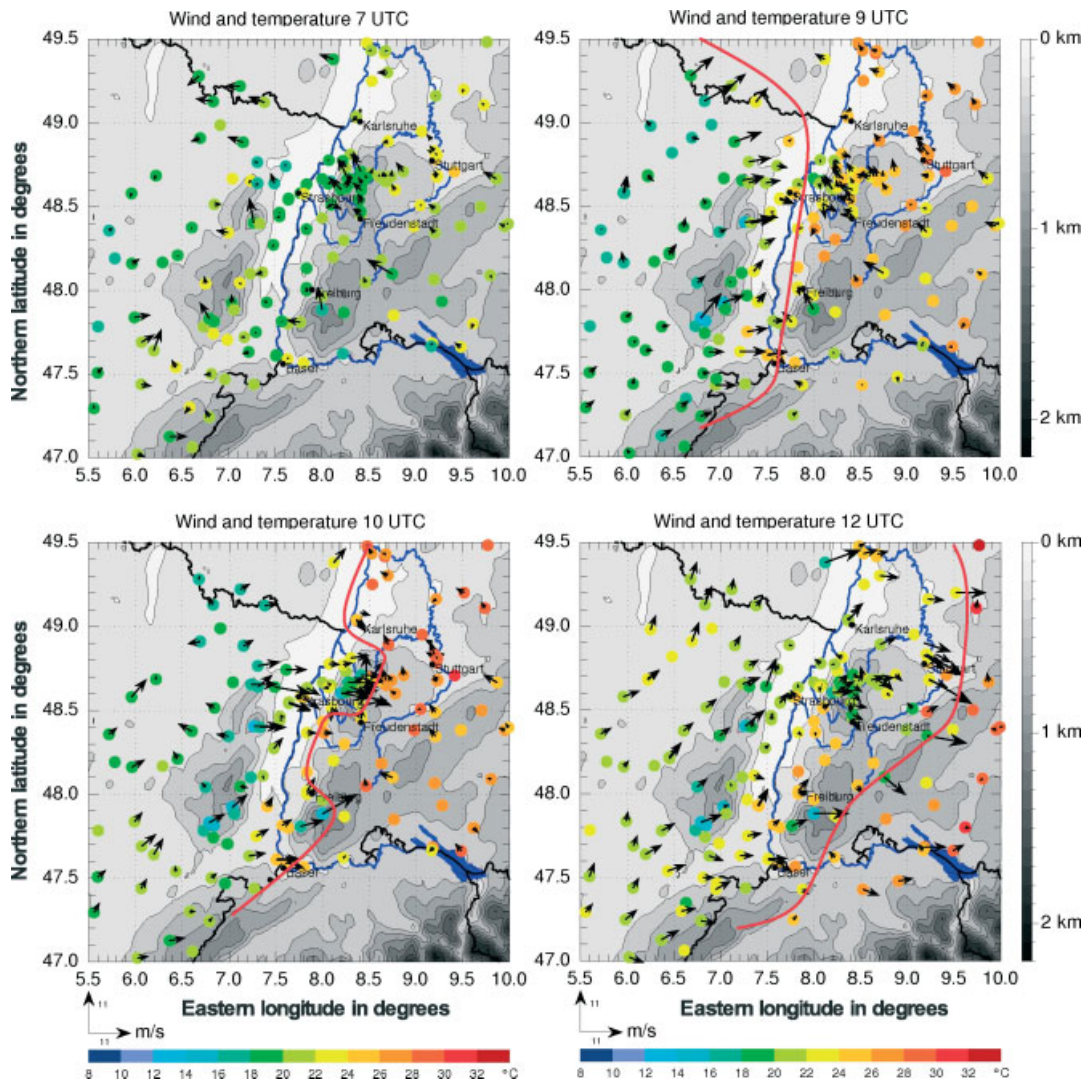
Figure 9. Near-surface wind and temperature in the COPS area taken from COPS and operational networks, valid for 20 July 2007 at 0700, 0900, 1000 and 1200 UTC. The red line indicates the position of the convergence line, modified partly (1000 and 1200 UTC) by the gust front over the northern Black Forest.

top more than 12 km height until 1135 UTC (Figure 15, lower right) and form a squall line with several embedded thunderstorms. The propagation between supersite H and radiosonde site Calw-Hirsau located 42 km east-northeast of supersite H (Figures 1 and 15, white square) is 10.7 m s^{-1}. This is only 1.5 m s^{-1} less than the propagation of the surface gust front between Hornisgrinde and Freudenstadt. After passing Calw-Hirsau at 1044 UTC, the gust front – squall line system is enhanced by additional convection forcing processes, such as strengthened horizontal convergence and free uplift, as the temperature exceeds T_c of 30.9°C (Figure 9). Between 1100 and 1200 UTC, individual cells within the squall line merge into one severe storm that now forms the southern end of the cold front of the meso-low over western Germany on a larger scale (Figures 4, 8 and 15). How can this fast development of deep convection be explained?

The main reasons are orographic lifting of the colder air above the surface layer and more humid air mass behind the gust front at the 1000 m steep slope of the Black Forest, in combination with forced and thermal lifting of the air downstream of the gust front over the mountains. Figure 16, showing the three-dimensional wind field measured by the research aircraft Do 128 above the Black Forest between

0747 and 0955 UTC, illustrates what happened. The view is from the southwest towards the Black Forest. The figure is a three-dimensional version of Figure 1. The vertical wind is given in colours and the horizontal wind by arrows. The flight track is explained in the figure caption.

There are three flight sections with significant mean upward vertical motion, indicating either lifting of the gust front air or lifting of the air ahead of the gust front. After take-off at 'Airbase' (0747 UTC), the western vertical profile P1 up to 2550 m amsl shows weak winds (3 m s^{-1}) from the southeast with low mean vertical motion (−0.5 m s^{-1}) and weak turbulence. During the following east–west oriented pattern flown from north to south between 0802 and 0925 UTC (Figures 1 and 16), the vertical motion stays calm, but the south-easterly wind increases to 12 m s^{-1} between 900 and 1500 m amsl, which is roughly 400 to 600 m above the terrain. The first feature of the arriving gust front is found in the southwestern part of the track at 0915 UTC and 1000 m amsl on the western slope of the Black Forest. The vertical wind speed in this section is up to + 3.0 m s^{-1}, the temperature is reduced by 5°C (not shown), and specific humidity increases from 10 to 13 g kg^{-1} (Figure 17).

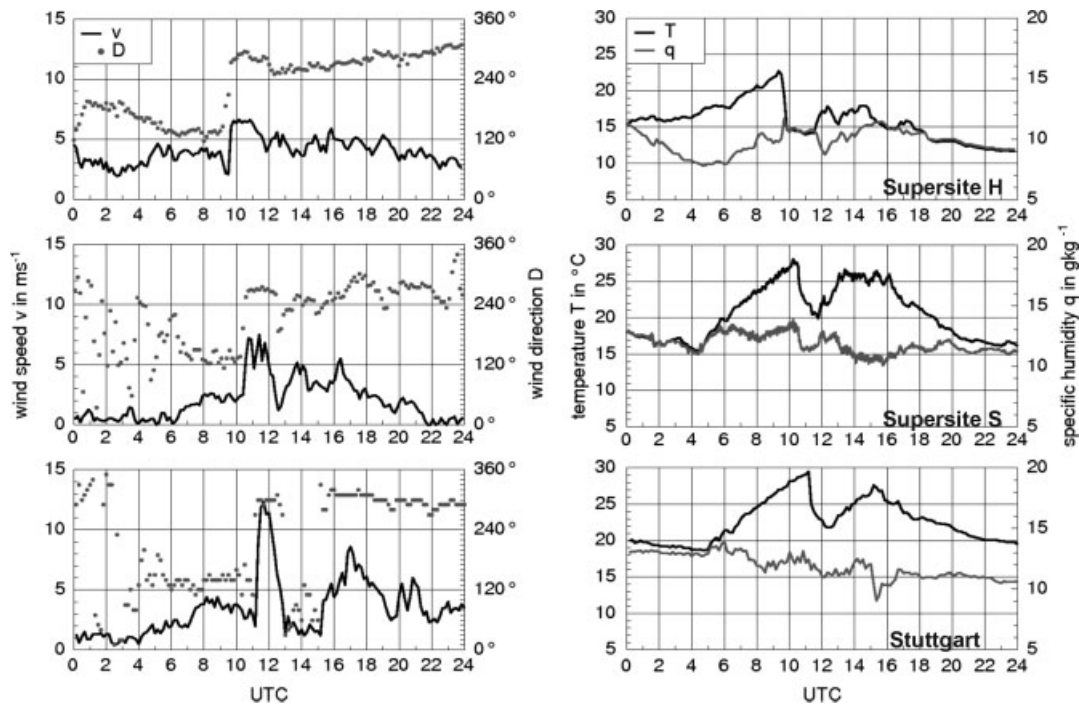Compared to the two western vertical profiles (P1, P2), the eastern profiles (P3, P4) flown between 0925 and 0940

Figure 10. Near-surface measurements of wind speed *v* and wind direction *D* (left), temperature *T* and specific humidity *q* (right) at supersite H (upper panel), supersite S (middle) and Stuttgart (lower panel). The figure explains the arrival of the gust front at the summit of the Hornisgrinde (supersite H) at 0933 UTC, its eastward propagation to supersite S (arriving at 1030 UTC) and its transformation to a fully developed convective cell passing Stuttgart (Figure 4, lower right) at 1130 UTC. The subsequent cold front arrives at 1515 UTC.

Table I. Convection-related indices prior to and after the gust-front passage.

	Supersite R	Supersite R	Supersite H	Supersite H	Calw-Hirsau	Calw-Hirsau
Gust-front passage	0908 UTC	1100 UTC	0808 UTC	1113 UTC	1010 UTC	1136 UTC
		0925 UTC		0933 UTC		1040 UTC
Launching relative to gust front	17 min prior	95 min after	85 min prior	100 min after	30 min prior	56 min after
CAPE in J kg^{-1}	223	2	717	–	2056	391
CIN in J kg^{-1}	449	71	76	–	22	101
Lifted Index in°C, Thunderstorm?	−2.4 possible, trigger needed	−0.1 possible, trigger needed	−3.8 probable	3.6 unlikely	−6.9 severe	−2.5 possible, trigger needed
LCL in m agl	365	653	972	803	1350	1037
LFC in m agl	3350	1880	1932	–	1866	2603
2 m temperature in°C	20.2	21.7	20.3	14.7	28.7	24.1
Convective temp. in°C	33.9	27.3	25.0	25.4	30.9	28.3
Vertical gradient of eq. pot. temp. Θ_{es} (saturated)	–	–	−25K/3000 m	−2K/3000 m	−60K/3000 m	−25K/3000 m

Calculated from radiosondes and surface data at supersites R (Rhine valley, 135 m amsl) and H (Hornisgrinde, 1163 m amsl), and at Calw-Hirsau (350 m amsl), 42 km east-northeast of Hornisgrinde (Figure 1).

UTC show that the wind in the lower 2950 m has turned from southeast to west-southwest and increased to over 12.0 m s^{-1}. The second section with positive mean vertical motion up to +2.0 m s^{-1} is on the descending profile P4 south of Freudenstadt between 0933 and 0940 UTC (Figures 16 and 18, right diagram). Synchronously with the high mean upward motion within the layer between 2250 and 1500 m amsl, the variance of the vertical wind is very low (weak turbulence), indicating larger-scale lifting of the air downstream of and above the gust front. Descending more between 1500 and 800 m amsl, the mean upward motion decreases below +1 m s^{-1}. At the same time, the turbulence increases significantly, the temperature decreases by 2.5°C, and the specific humidity increases from 7 to 10 g kg^{-1}
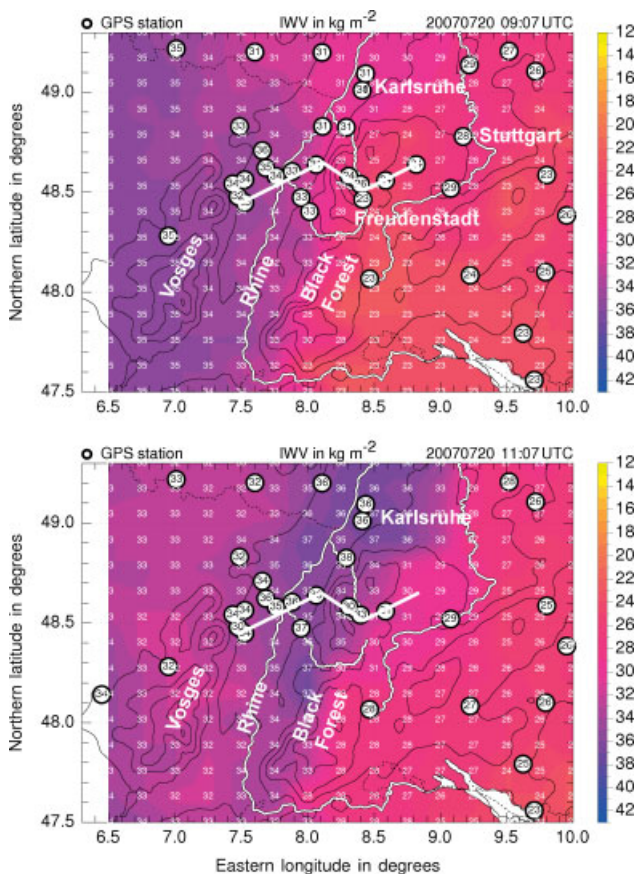
Figure 11. Integrated water vapour at GPS stations (IWV in kg m^{-2}, white circles) at 0907 UTC (top) and at 1107 UTC (bottom) with interpolated IWV data for the outer COPS area (colour code). Black solid lines indicate the orography, and the white line shows the line of supersites.

Figure 12. Vertical profiles of wind speed (top panel, colours), wind direction (top panel, arrows), and vertical wind speed (2nd panel) measured by a UHF radar wind profiler on 20 July 2007 at supersite R in the Rhine valley between 0900 and 1200 UTC to show the arrival of the gust front. The black colour in the 2nd panel indicates showers. Time evolution of the range-corrected signal at 1064 nm (3rd panel) and water vapour mixing ratio (bottom panel) measured by the co-located Raman lidar system BASIL. The sequences A to E are discussed in the text. Black colour in the range-corrected signal represents cloud bases.

(Figures 17 and 18). This is the boundary-layer air over the mountain plateau, but not the gust front air, because the wind is still from a southerly direction on this level at this time.

Finally, flying northbound and at a low level through the Murg valley, a down-valley southerly wind is measured. Reaching the valley entrance in the north (Figure 1, Ger) the wind turns within seconds to westerly at 20.0 m s^{-1}, and 9.0 m s^{-1} upward motion. Vigorous turbulence occurs suddenly when the gust front at 0944 UTC enters the northern part of the Murg valley. The mission had to be cancelled because of dangerous turbulence.

The different air masses passed through by the Do 128 during this mission can be separated clearly by the measurements of the mixing ratio (Figure 17, same pattern as Figure 16). Above the PBL over the mountains during the whole flight, the mixing ratio is uniformly between 6.0 and 7.5 g kg^{-1}, as seen on the vertical profiles P1 to P4, although the wind turns between the western (P1, P2) and the eastern profiles (P3, P4) by 90° at the minimum. When penetrating the mountainside PBL, the mixing ratio increases to 10 g kg^{-1} (Figures 17 and 18: P4 at 1350 m amsl). Finally, when the flight passes the gust front air after the cancellation point, the mixing ratio rises to 15 g kg^{-1}, a similar level as seen in the south-western part of the pattern at 0915 UTC.

These findings clearly indicate that the gust front air reaches the Hornisgrinde at its southern (0915 UTC) and northern (0940 UTC) edge and flows over the central part
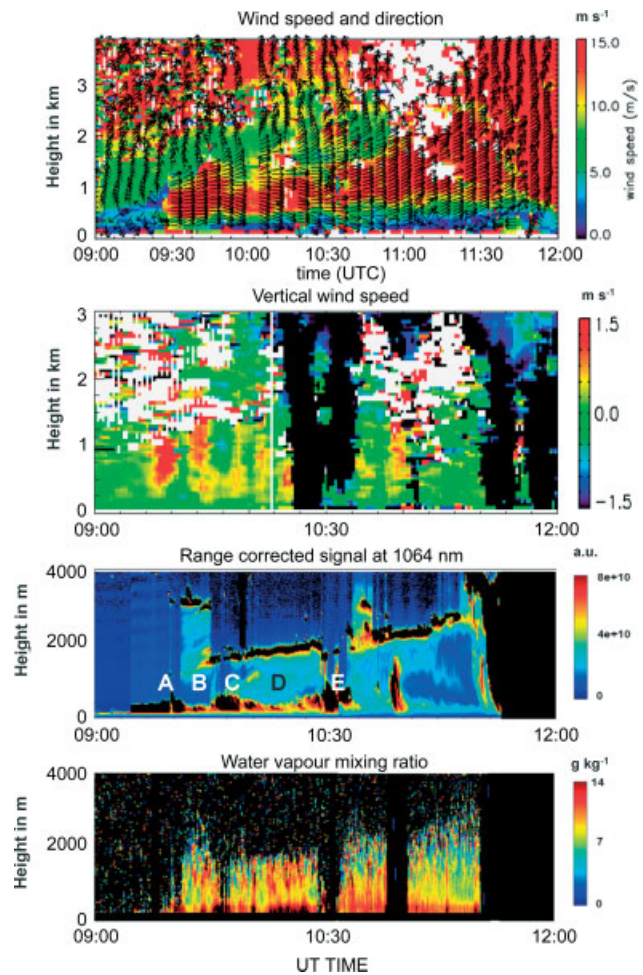
of the mountain by forced lifting of 1000 m. Downstream of the gust front, prior to its arrival over the northern Black Forest, the air is lifted by about 3000 m within 2000 s. This can be estimated as follows: the upward motion in the P4 profile (Figure 16) starts at approximately 0933 UTC, the same time as when the gust front reaches H. The horizontal distance between H and the location of the profile is 25 km and the propagation speed of the gust front is 12 m s^{-1}. Hence, the gust front needs 2100 s to propagate to the location where the profile is flown. During this time, a mean vertical motion of 1.5 m s^{-1} is observed, which results in wedge-shaped lifting of the air mass of 3150 m, roughly from the western Black Forest crest (supersite H) up to 4000 m amsl, the level where the first showers are observed at 1000 UTC (Figure 15, top left). In cases of westerly flow, the western crest of the Black Forest was identified to be a trigger line for boundary-layer modifications and enhanced vertical air mass exchange (Corsmeier *et al.*, 1994). This analysis shows that CI happened mainly between 0915 and 0940 UTC within the warmer air mass downstream of the gust front rather than within the colder (and humid only between 2000 and 3000 m amsl) gust front air. Due to
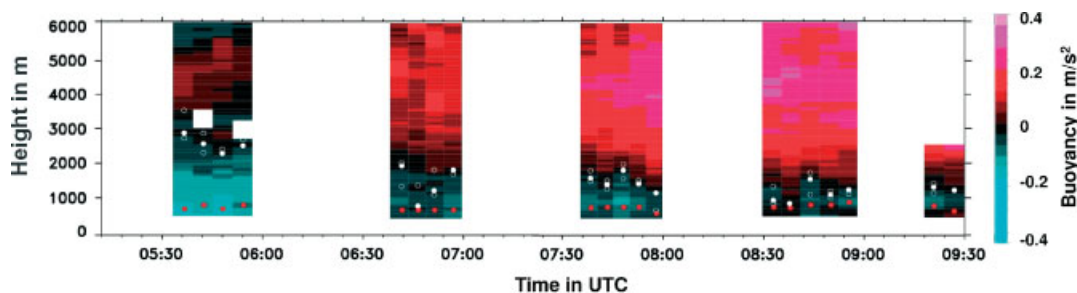
Figure 13. Profiles of buoyancy *B* in the morning of 20 July 2007, calculated from water vapour differential absorption lidar (DIAL) and rotational Raman lidar at mountain supersite H (Figure 1) before the gust front arrived. Red dots indicate the lifting condensation level (LCL), white dots the level of free convection (LFC), and white circles the uncertainty of LFC (±1 sigma).
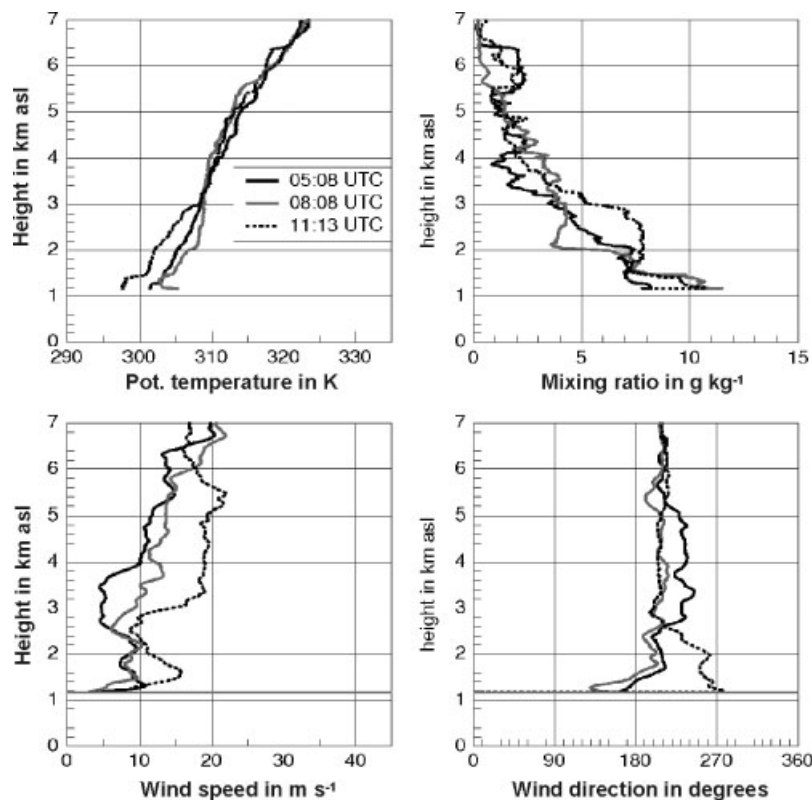

Figure 14. Vertical soundings at the summit supersite H before (0508 and 0808 UTC) and after (1113 UTC) the passage of the gust front on 20 July 2007.

an enhanced horizontal temperature gradient, a thermally direct circulation develops: warm air is lifted and cold air is lowered, and at first a convergence line (1000 UTC) and later a squall line (1100 UTC) is generated.

The impacts of lifting and the passage of the gust front on atmospheric stratification and the initiation of deep convection are reflected by convection-related indices calculated from vertical profiles prior to and behind the gust front at supersites R and H and at radiosonde site Calw-Hirsau, and by the corresponding vertical gradients of the equivalent potential temperature Θ_{es} (Table I). CAPE is significantly increased prior to the gust-front passage within two hours between R, H and Calw-Hirsau from 223 to 717 to 2056 J kg^{-1}, while CIN (more locally influenced and due to the diurnal cycle) is reduced from 449 to 76 to 22 J kg^{-1}. This favours the development of deep convection, increasing from west to east. The LCL is 365 m agl at supersite R, 972 m agl at supersite H, and 1350 m at Calw-Hirsau and the LFC is 3350 m agl at supersite R and about 1900 m agl at the other two sites. The LCL can be overcome easily at the eastern two sites by the forced vertical lifting mentioned above,

but not at supersite R because of insufficient lifting. The convective temperature is not reached at any site, showing that in this stage there is no direct thermal trigger for convection. Finally, there is a probability of deep convection and thunderstorms at supersite H and severe thunderstorms at Calw-Hirsau prior to the gust front, but not at supersite R in the Rhine valley. This probability at supersite H and Calw-Hirsau is reduced behind the gust front, as can be seen by the reduced CAPE, enhanced CIN, and Lifted Index.

The possibility of vertical stratification becoming unstable and releasing CAPE is shown by the vertical profiles of Θ and Θ_{es} in the lower 3000 m agl (Table I). While at supersite H and Calw-Hirsau prior to and behind the gust front, the Θ profiles are neutral within the PBL and stable above, the Θ_{es} vertical gradient at H is -25 K/3000 m. The potential instability (if saturated) increases up to $\Theta_{es} = -60$ K/3000 m when moving eastward to Calw-Hirsau. After the gust-front passage, the values are reduced to $\Theta_{es} = -2$ K/3000 m at H and to $\Theta_{es} = -25$ K/3000 m at Calw-Hirsau. This is another clear signal for the potential of the air mass to develop deep convection and severe thunderstorms, if
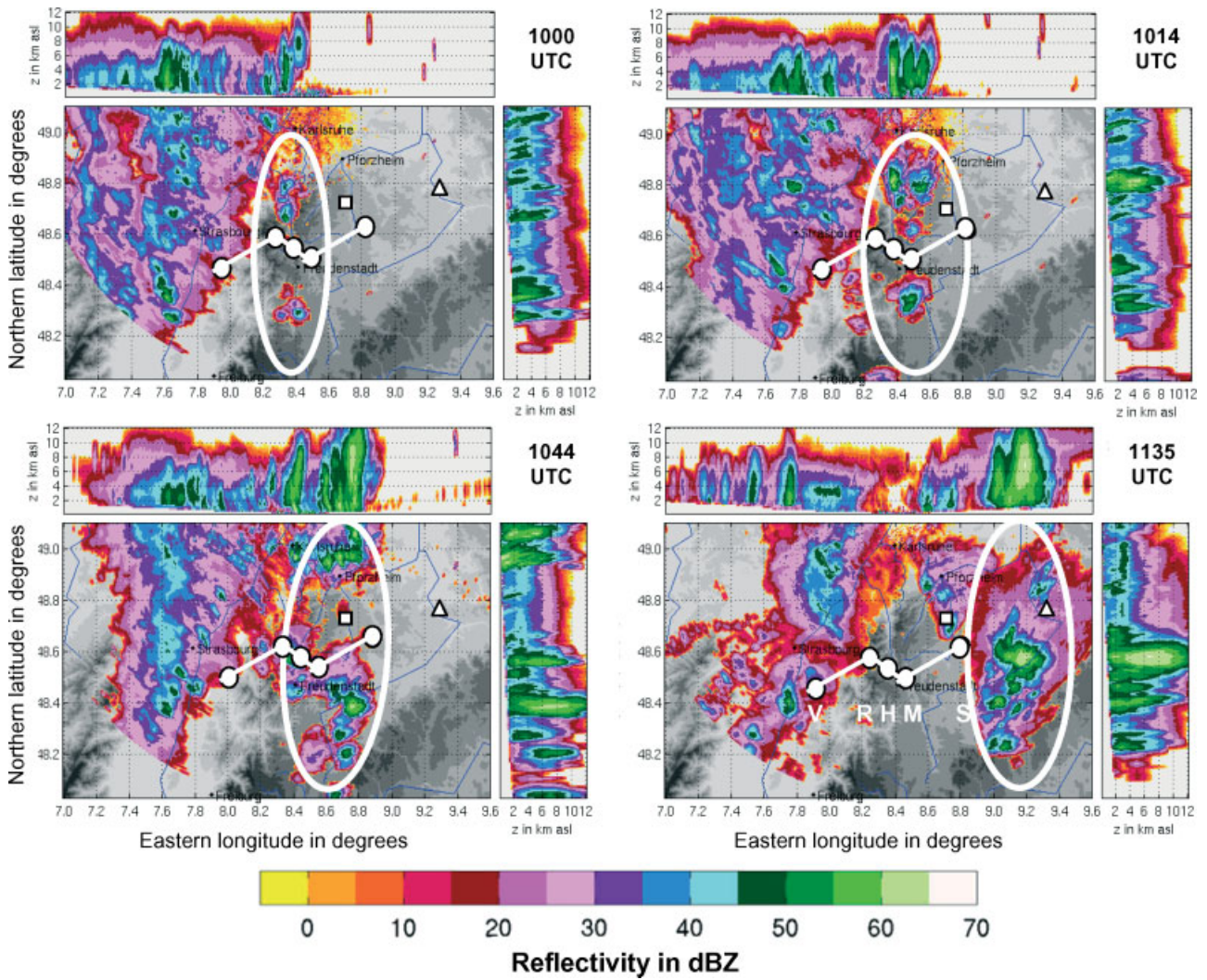
Figure 15. Hydrometeor reflectivity in the inner COPS area, when the gust front passes between 1000 and 1135 UTC, seen from the radar at KIT in Karlsruhe. The vertical extension of the convective cells is shown above and to the right-hand side of the x–y diagram. The cross sections are not taken at specific longitudes and latitudes. They are accumulated reflectivities in east-west and north-south direction, respectively. Sites discussed are given by white symbols: Calw-Hirsau (square), line of supersites V-R-H-M-S (circles) and Stuttgart (triangle). The white oval shows the gust front – squall line system.
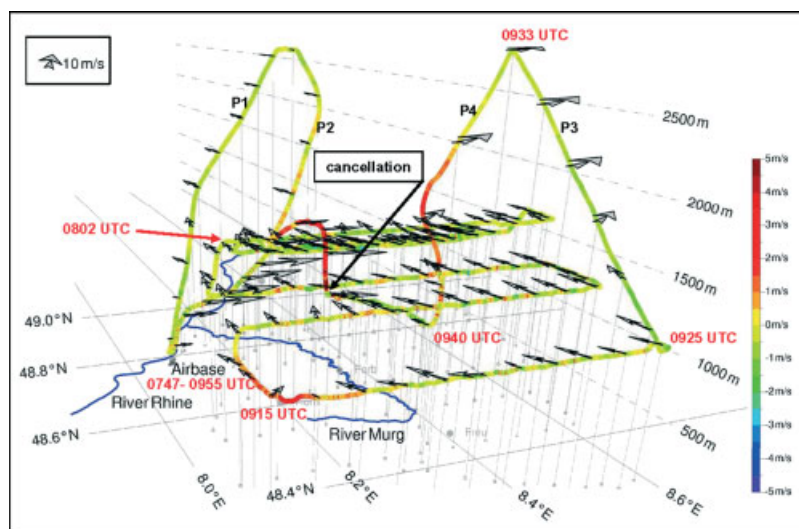

Figure 16. Three-dimensional extension of Figure 1. Vertical wind speed (colours) and wind direction (arrows) along the flight pattern of the Do 128 aircraft above the northern Black Forest (inner COPS area) on 20 July 2007, between 0747 and 0955 UTC. Take-off and touchdown at 'Airbase'. View from the southwest onto the northern Black Forest. The flight started with the two western vertical profiles up to 2500 m amsl (P1, P2) followed by the east–west oriented horizontal legs from north to south between 900 and 1400 m amsl, the two eastern vertical profiles up to 2950 m amsl (P3, P4), and the lowest-level flight through the Murg valley northward between 900 and 600 m amsl (mark: cancellation). Details are given in the text.
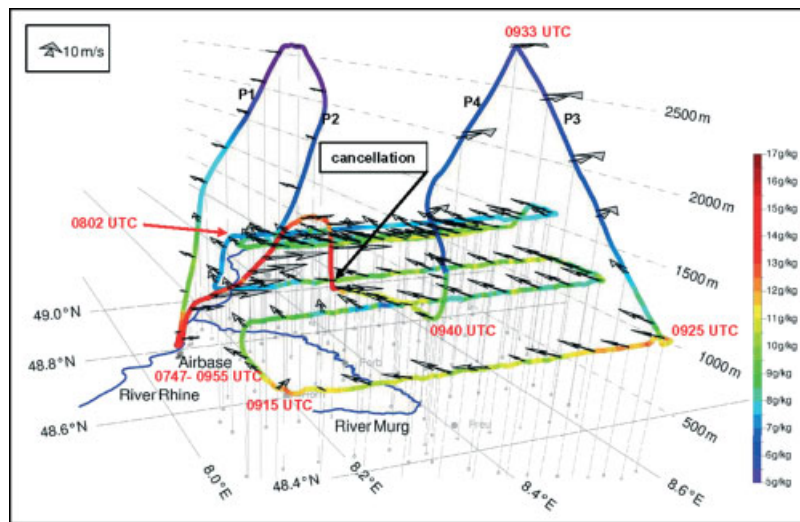
Figure 17. The same as Figure 16 but for mixing ratio (colour coded).
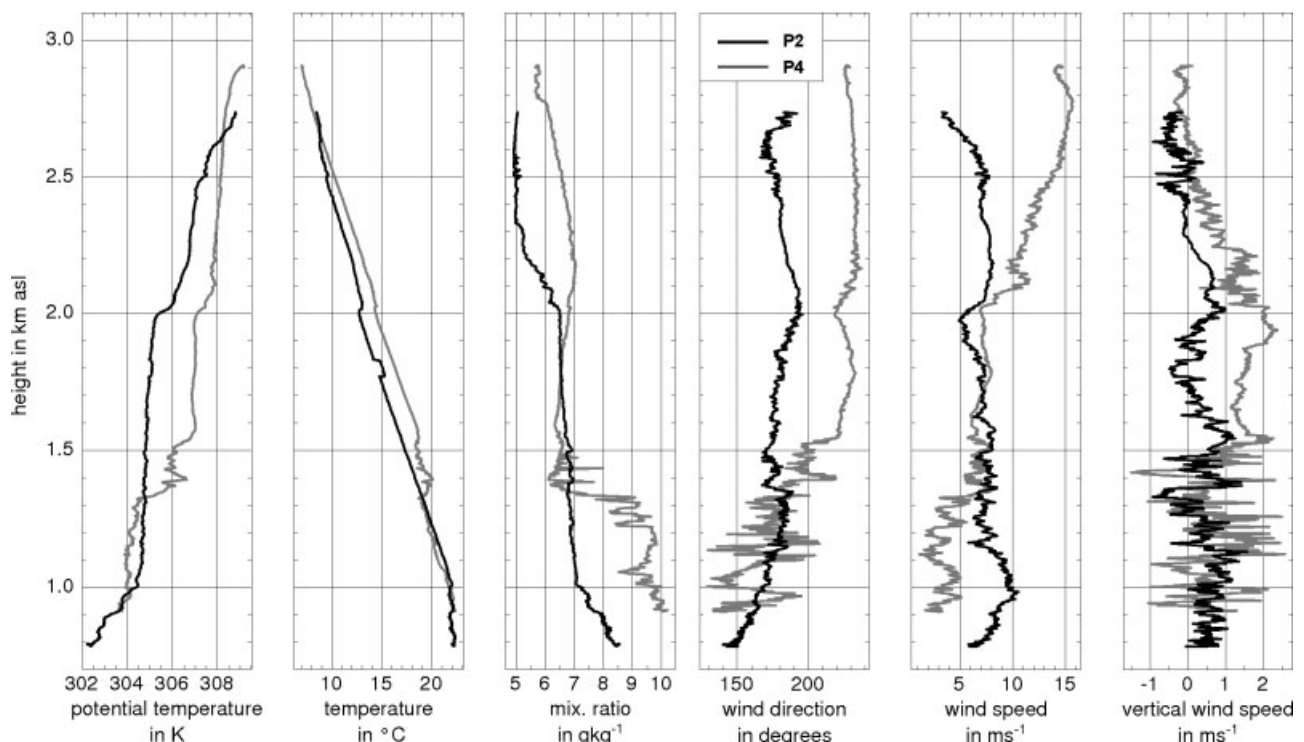

Figure 18. Vertical profiles of wind, temperature and humidity measured aboard the Do 128 above the northern Black Forest between 800 and 2950 m amsl. The descending profile in black (P2 in Figures 16 and 17) is flown in the northwestern part of the track between 0757 and 0802 UTC. The descending profile in grey (P4 in Figures 16 and 17) is flown in the central part of the Black Forest near Freudenstadt between 0933 and 0940 UTC.

sufficient forced lifting activates the potential instability. This is what happened between 1000 and 1200 UTC in the eastern COPS area.

3.5. Convection-related precipitation pattern

The precipitation pattern resulting from this weather episode clearly reflects the different, scale-dependent precipitation-generating processes. Figure 4 (visible-light (VIS) satellite images), Figure 8 (DWD precipitation radar composite), Figure 15 (Institute for Meteorology and Climate Research, Karlsruhe Institute of Technology (IMK) precipitation radar sequence), and Figure 19 (VERA precipitation analysis) provide insight into the temporal and spatial evolution of

precipitation, its amount and location. The precipitation distribution on the synoptic scale is shown in Figures 8 and 19. Figure 8 depicts the momentary reflectivity at 1200 UTC from the DWD radar network. A band of light rain stretching from Belgium over western Germany to the Rhine valley (blue colours) is associated with lifting at the cold front of the weak low-pressure system. Prior to the cold front, especially over the COPS area and north of it along the convergence line, cells with high reflectivity develop (yellow and red colours), indicating deep convection and heavy precipitation. The precipitation diagram demonstrates the decay of the southern part of the cold front in the Rhine valley and its redevelopment triggered by the gust front, the orography and the convergence line when passing the

Black Forest towards the east. Figure 19 (upper panel) shows the rain total in the outer COPS area between 0600 and 1200 UTC, interpolated by VERA on an 8 km grid. The highest amount of rain (10 mm) is measured in the morning (0600 until 0700 UTC) below the decaying core of the MCS in northern France (Figure 4, upper row), and widespread precipitation between 3 and 8 mm is found over large areas of north-eastern France, mainly coupled with the developing cold front. When passing the Vosges towards the east, precipitation stops over the Rhine Valley between 1000 and 1100 UTC (Figure 19, middle). The first showers of the developing prefrontal line of deep convection are detected south of Karlsruhe (approx. 1.5 mm). This is in accordance with the reflectivity measured by the KIT radar in Karlsruhe, which indicates a line of showers south of Karlsruhe and a little east of the crest of the Black Forest (Figure 15, upper row). The very first reflectivity signals are restricted to upper levels (>4 km). This confirms the finding that the warm und relatively humid air ahead of the gust front is strongly lifted by the dynamics of this air mass and by forced lifting due to orography. Convection and subsequent showers therefore start in the middle troposphere without reaching the surface. Parallel to the strengthening of deep convection within the pre-gust-front air (Figure 15), precipitation is enhanced between 1100 and 1200 UTC (Figure 19, bottom). Southwest of Stuttgart, up to 9 mm of rain are measured during the severe thunderstorm shown in Figure 15 (1135 UTC). Figure 19 clearly shows the reorganisation of the precipitation pattern governed by the frontal system and its convergence line. In the western COPS area and north of it, precipitation along the frontal system decays rapidly. There is no more rain after 1100 UTC. More or less synchronously, convection starts a little east of the crest of the northern Black Forest and develops to deep convection with heavy showers east of the Black Forest. This results in an area free of precipitation and in a large part free of clouds over the mountains between 1100 and 1200 UTC (Figure 4, 1130 UTC; Figure 19, bottom).

4.   Summary and conclusions

As regards the initiation of convection, the COPS IOP 9c is characterised by a complex interaction of convection-driving forces of different scales. The central feature is a two-way interaction of processes initiating convection: from larger and longer scales in time and space down to smaller and shorter scales and back to longer and larger ones.

Large-scale lifting driven by positive vorticity advection and warm air advection generates the weak surface low over France. Within the warm sector of the low an MCS develops during the night and moves towards the northeast near the western COPS area. Later on, the MCS generates a second weak core of the low over Belgium and its easterly outflow over the Vosges initiates a gust front roughly 60 km wide which propagates rapidly in an easterly direction. When passing the Vosges in the early morning, two sequences of deep convective clouds with moderate showers are initiated with a lifetime of about 90 minutes. During the passage of the Rhine valley, the gust front undergoes subsidence. This inhibits the development of new convection, and advected clouds are dissolved.

The following complex process of convection initiation is broken down into individual steps. The advantageous interaction of the individual steps in time and space are
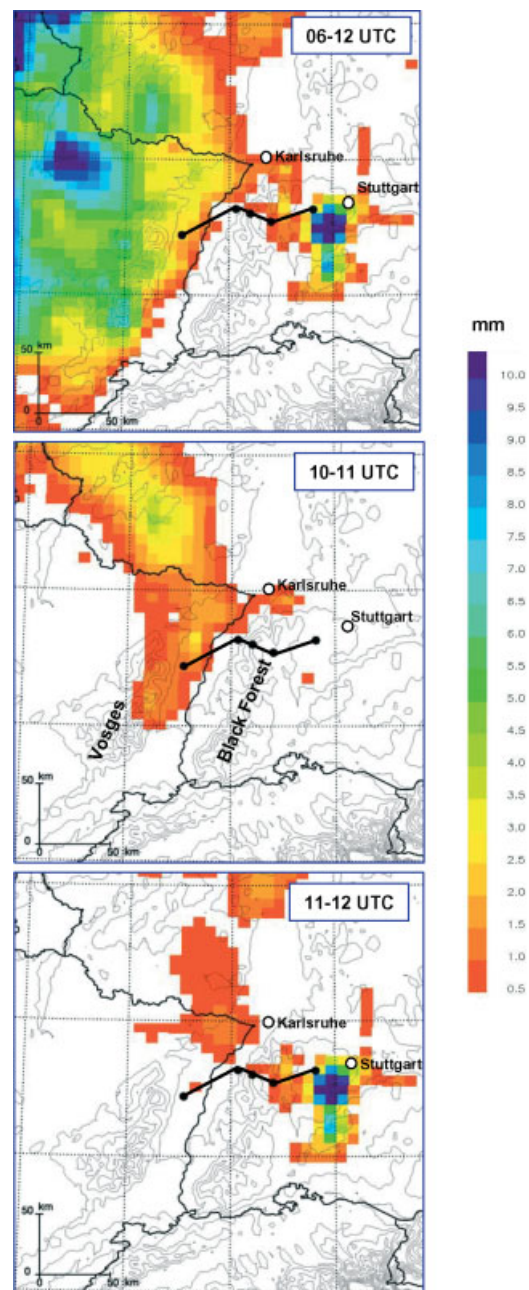

Figure 19. Measured precipitation in the outer COPS area on 20 July 2007. Accumulated data from 0600 to 1200 UTC (top), from 1000 to 1100 UTC (middle), and from 1100 to 1200 UTC (bottom). The measurements are interpolated by the VERA method on an 8 km grid.

responsible for CI and the subsequent deep convection and convective storms.

- The flow (gust front generated by the MCS) undergoes forced lifting at a low mountain range (Black Forest).
- The warm and humid air ahead of the gust front (above the Black Forest) is initially lifted by the gust front air due to severe convergence.
- This is the time when CI occurs within the lifted air prior to and above the gust front. First showers are observed.
- Due to synoptic reasons (cloud systems of the MCS, and clear sky downstream in the east) and the daily cycle (daytime episode), the development of a convergence line ahead of the gust front.

- Generation of a direct thermal circulation at the gust front – convergence line system. Further lifting of warm downstream air and subsidence of cold gust-front air.
- Destabilisation of the air ahead of the convergence line. Later (after noon) the convective temperature in the eastern COPS area is exceeded and enhancement of CI occurs.
- Rapid generation of deep convection at the convergence line. Development of individual convective cells: transformation of the convergence line into a squall line.

The first three points are governed by larger-scale processes (synoptic scale) and orography. The last four points depend on synoptic preconditions and daytime (global radiation). Finally, the cells merge into a new MCS east of the COPS area. Meanwhile, the low-pressure system over France, Belgium and the Channel has formed a cold front stretching from the Channel to the eastern COPS area on the synoptic scale. The new MCS is part of this cold front and moves further to the east. This case demonstrates:

- the importance of scale interaction to convection-driving processes and
- the existence of a two-way scale interaction from large to small scales and vice versa.

Downscaling is analysed in the chain of processes from the MCS over France generating the regional-scale gust front and finally causing local-scale CI by forced lifting. From then on, CI is enhanced by upscaling: Locally triggered cells are amplified in the environment of the convergence line, a squall line is triggered, and finally single storms merge along the synoptic-scale cold front into a new MCS. On the local scale, it is important that CI takes place significantly before the first visible sign of any convective phenomena (clouds, showers, lightning). In cases of non-negligible basic flow, the locations of CI and the area of highest convective activity were significantly apart from each other. In other cases, without a significant basic flow, CI can be detected by stationary convective clouds within a diurnal cycle.

During COPS IOP 9c, the initiation of convection was governed by a bi-directional interaction of atmospheric flow systems of different scales: from cyclogenesis on the synoptic scale to MCS and cold-front formation on the mesoscale, and the development of a gust front, a convergence line and a squall line on the regional scale, down to orographically and thermally driven circulations on the local scale. Due to the interplay of different processes, weather phenomena are modified: (i) the gust front – convergence line interaction finally forms a squall line and single storms, (ii) the MCS generates a meso-low over Belgium and partly modifies the cold front of the low outside the COPS area north of the squall line, and (iii) the gust front flow over a pronounced ridge–valley–ridge system initiates and dissolves/suppresses convection depending on orography and daytime.

This case of CI, governed by scale interaction, is a great challenge for forecasting the resulting weather. This applies to nowcasting tools using on-line observational data as well as to forecasting of such processes by high-resolution operational models. The performance of the COSMO-DE model of the DWD in this case will be highlighted in a subsequent paper.

References

Aoshima F, Behrendt A, Bauer H-S, Wulfmeyer V. 2008. Statistics of convection initiation by use of Meteosat rapid scan data during the Convective and Orographically-induced Precipitation Study (COPS). *Meteorol. Z.* **17**: 921–930.

Barthlott C, Corsmeier U, Meißner C, Braun F, Kottmeier C. 2006. The influence of mesoscale circulation systems on triggering convective cells over complex terrain. *Atmos. Res.* **81**: 150–175.

Behrendt A, Pal S, Aoshima F, Bender M, Blyth A, Corsmeier U, Cuesta J, Dick G, Dorninger M, Flamant C, Di Girolamo P, Gorgas T, Huang Y, Kalthoff N, Khodayar S, Mannstein H, Träumner K, Wieser A, Wulfmeyer V. 2011. Observation of convection initiation processes with a suite of state-of-the-art research instruments during COPS-IOP 8b. *Q. J. R. Meteorol. Soc.* **137**(S1): 81–100, DOI: 10.1002/qj.758.

Browning KA, Ludlam FH. 1962. Airflow in convective storms. *Q. J. R. Meteorol. Soc.* **88**: 117–135.

Behrendt A, Wulfmeyer V, Riede A, Wagner G, Pal S, Bauer H, Radlach M, Späth F. 2009. 3-Dimensional observations of atmospheric humidity with a scanning differential absorption lidar. *Proc. SPIE* **7475**: 74750L, DOI: 10.1117/12.835143.

Browning KA, Blyth AM, Clark PA, Corsmeier U, Morcrette CJ, Agnew JL, Ballard SP, Bamber D, Barthlott C, Bennett LJ, Beswick KM, Bitter M, Bozier KE, Brooks BJ, Collier CG, Cook C, Davies F, Deny B, Dixon MA, Feuerle T, Forbes RM, Gaffard C, Gray MD, Hankers R, Hewison TJ, Kalthoff N, Khodayar S, Kohler M, Kottmeier C, Kraut S, Kunz M, Ladd DN, Lean HW, Lenfant J, Li Z, McGregor J, Marsham J, Mobbs SD, Nicol J, Norton EG, Parker DJ, Perry F, Ramatschi M, Ricketts HMA, Roberts NM, Russell A, Schulz H, Slack EC, Vaughan G, Waight J, Wareing DP, Watson RJ, Webb AR, Wieser A. 2007. The Convective Storms Initiation Project. *Bull. Am. Meteorol. Soc.* **88**: 1939–1955.

Corsmeier U, Koßmann M, Vögtlin R, Fiedler F. 1994. 'Water vapour transport by stationary convective cells over hilly terrain.' Pp 761–765 in *Proceedings of EUROTRAC Symposium 1994,* Borrell PM (ed). SPB Academic Publishing BV: The Hague.

Di Girolamo P, Summa D, Ferretti R. 2009. Multiparameter Raman lidar measurements for the characterization of a dry stratospheric intrusion event. *J. Atmos. Oceanic Technol.* **26**: 1742–1762.

Fiedler F, Bischoff-Gauß I, Kalthoff N, Adrian G. 2000. Modeling of the transport and diffusion of a tracer in the Freiburg-Schauinsland area. *J. Geophys. Res.* **105**: 1599–1610.

Groenemeijer P, Barthlott C, Behrendt A, Corsmeier U, Handwerker J, Kohler M, Kottmeier C, Mahlke H, Pal S, Radlach M, Trentmann J, Wieser A, Wulfmeyer V. 2008. Observations of kinematics and thermodynamic structure surrounding a convective storm cluster over a low mountain range. *Mon. Weather Rev.* **137**: 585–602.

Hasel M. 2006. '*Strukturmerkmale und Modelldarstellung der Konvektion über Mittelgebirgen.*' PhD Thesis, Wissenschaftliche Berichte des Instituts für Meteorologie und Klimaforschung, Universität Karlsruhe, Nr. 39, ISSN 0179–5619.

Hasel M, Kottmeier C, Corsmeier U, Wieser A. 2005. Airborne measurements of turbulent trace gas fluxes and analysis of eddy structure in the convective boundary layer over complex terrain. *Atmos. Res.* **74**: 381–402.

Kalthoff N, Vogel B. 1992. Counter-current and channelling effect under stable stratification in the area of Karlsruhe. *Theor. Appl. Climatol.* **45**: 113–126.

Kalthoff N, Horlacher V, Corsmeier U, Volz-Thomas A, Kolahgar B, Geiß H, Möllmann-Coers M, Knaps A. 2000. Influence of valley winds on transport and dispersion of airborne pollutants in the Freiburg-Schauinsland area. *J. Geophys. Res.* **105**: 1585–1597.

Kalthoff N, Adler B, Barthlott C, Corsmeier U, Mobbs SD, Crewell S, Träumner K, Kottmeier C, Wieser A, Smith V, Di Girolamo P. 2009. The impact of convergence zones on the initiation of deep convection: A case study from COPS. *Atmos. Res.* **93**: 680–694.

Kalthoff N, Kohler M, Barthlott C, Mobbs SD, Corsmeier U, Adler B, Träumner K, Foken T, Eigenmann R, Krauss L, Khodayar S, Di Girolamo P. 2011. The dependence of convection-related parameters on surface and boundary-layer conditions over complex terrain. *Q. J. R. Meteorol. Soc.* **137**(S1): 70–80, DOI: 10.1002/qj.686.

Koßmann M, Fiedler F. 2000. Diurnal momentum budget analysis of thermally induced slope winds. *Meteorol. Atmos. Phys.* **75**: 195–215.

Koßmann M, Vögtlin R, Corsmeier U, Vogel B, Fiedler F, Binder H-J, Kalthoff N, Beyrich F. 1998. Aspects of the convective boundary layer structure over complex terrain. *Atmos. Environ.* **32**: 1323–1348.

Kottmeier C, Kalthoff N, Corsmeier U, Barthlott C, van Baelen J, Behrendt A, Behrendt R, Blyth A, Coulter R, Crewell S, Di Girolamo P, Dorninger M, Flamant C, Foken T, Hagen M, Hauck C, Höller H, Konow H, Kunz M, Mahlke H, Mobbs SD, Richard E, Steinacker R, Weckwerth TM, Wieser A, Wulfmeyer V. 2008. Mechanisms initiating deep convection over complex terrain during COPS. *Meteorol. Z.* **17**: 931–948.

Kurz M. 1990. '*Leitfäden für die Ausbildung im Deutschen Wetterdienst, Nr. 8: Synoptische Meteorologie, 2. Auflage.*' Selbstverlag des Deutschen Wetterdienstes: Offenbach am Main.

Marsham JH, Blyth AM, Parker DJ, Beswick K, Browning KA, Corsmeier U, Kalthoff N, Khodayar S, Morcrette CJ, Norton EG. 2007. Variable cirrus shading during CSIP IOP 5. II: Effects on the convective boundary layer. *Q. J. R. Meteorol. Soc.* **133**: 1661–1675.

Meißner C, Kalthoff N, Kunz M, Adrian G. 2007. Initiation of shallow convection in the Black Forest mountains. *Atmos. Res.* **86**: 42–60.

Norton EG, Vaughan G, Methven J, Coe H, Brooks B, Gallagher M, Longley I. 2006. Boundary layer structure and decoupling from synoptic scale flow during NAMBLEX. *Atmos. Chem. Phys.* **6**: 433–445.

Radlach M, Behrendt A, Wulfmeyer V. 2008. Scanning rotational Raman lidar at 355 nm for the measurement of tropospheric temperature fields. *Atmos. Chem. Phys.* **8**: 159–169.

Schwitalla T, Bauer H-S, Wulfmeyer V, Aoshima F. 2011. High-resolution simulation over central Europe: assimilation experiments during COPS IOP9c. *Q. J. R. Meteorol. Soc.* **137**(S1): 156–175, DOI: 10.1002/qj.721.

Steinacker R, Ratheiser M, Bica B, Chimani B, Dorninger M, Gepp W, Lotteraner C, Schneider S, Tschannett S. 2006. A mesoscale data analysis and downscaling method over complex terrain. *Mon. Weather Rev.* **134**: 2758–2771.

Weckwerth TM. 2000. The effect of small-scale moisture variability on thunderstorm initiation. *Mon. Weather Rev.* **128**: 4017–4030.

Weckwerth TM, Parsons DB, Koch SE, Moore JA, LeMone MA, Demoz BB, Flamant C, Geerts B, Wang J, Feltz WF. 2004. An overview of the international H_2O project (IHOP$_{2002}$) and some preliminary highlights. *Bull. Am. Meteorol. Soc.* **85**: 253–277.

Wilson JW, Roberts RD. 2006. Summary of convective storm initiation and evolution during IHOP: Observational and modeling perspective. *Mon. Weather Rev.* **134**: 23–47.

Wulfmeyer V, Behrendt A. 2007. '*Convective and Orographically-induced Precipitation Study, COPS Field Report 2.1.*' Available at: https://www.uni-hohenheim.de/spp-iop/further_reading/further_reading.htm.

Wulfmeyer V, Behrendt A, Bauer H-S, Kottmeier C, Corsmeier U, Blyth A, Craig G, Schumann U, Hagen M, Crewell S, Di Girolamo P, Flamant C, Miller M, Montani A, Mobbs SD, Richard E, Rotach MW, Arpagaus M, Russchenberg H, Schlüssel P, König M, Gärtner V, Steinacker R, Dorninger M, Turner DD, Weckwerth TM, Hense A, Simmer C. 2008. The Convective and Orographically-induced Precipitation Study: A research and development project of the World Weather Research Program for improving quantitative precipitation forecasting in low-mountain regions. *Bull. Am. Meteorol. Soc.* **89**: 1477–1486.

Wulfmeyer V, Behrendt A, Kottmeier C, Corsmeier U, Barthlott C, Craig G, Hagen M, Althausen D, Aoshima F, Arpagaus M, Bauer H-S, Bennett L, Blyth A, Brandau C, Champollion C, Crewell S, Dick G, Di Girolamo P, Dorninger M, Dufournet Y, Eigenmann R, Engelmann R, Flamant C, Foken T, Gorgas T, Grzeschik M, Handwerker J, Hauck C, Höller H, Junkermann W, Kalthoff N, Kiemle C, Klink S, König M, Krauss L, Long C, Madonna F, Mobbs SD, Neininger B, Pal S, Peters G, Pigeon G, Richard E, Rotach MW, Russchenberg H, Schwitalla T, Smith V, Steinacker R, Trentmann J, Turner DD, van Baelen J, Vogt S, Volkert H, Weckwerth TM, Wernli H, Wieser A, Wirth M. 2011. The Convective and Orographically-induced Precipitation Study (COPS): The scientific strategy, the field phase, and research highlights. *Q. J. R. Meteorol. Soc.* **137**(S1): 3–30, DOI: 10.1002/qj.752.

Wulfmeyer V, Bösenberg J. 1996. Single-mode operation of an injection-seeded alexandrite ring laser for application in water vapor and temperature differential absorption lidar. *Opt. Lett.* **21**: 1150–1152.